Evidences of metasomatism and refertilization in West Eifel and Siebengebirge Sub-Continental Lithospheric Mantle: clues from volatiles in fluid inclusions and petrology of ultramafic xenoliths

Andrea Luca Rizzo[a,b], Barbara Faccini[b], Federico Casetta[b,*], Luca Faccincani[b], Theodoros Ntaflos[c], Francesco Italiano[a], Massimo Coltorti[a,b]

[a] *Sezione di Palermo, Istituto Nazionale di Geofisica e Vulcanologia, Via Ugo La Malfa 153, 90146 Palermo, Italy*

[b] *Department of Physics and Earth Sciences, University of Ferrara, Via Saragat 1, 44121 Ferrara, Italy*

[c] *Department of Lithospheric Research, University of Vienna, Althanstraße 14, 1090 Vienna, Austria*

*** Corresponding author:** Federico Casetta, PhD; email: cstfrc@unife.it

Abstract

The possibility of constraining the nature and evolution of specific portions of the Sub-Continental Lithospheric Mantle (SCLM) by means of an integrated study of petrography, mineral chemistry and volatiles concentration in fluid inclusions (FI) is a frontier approach that can provide clues on the volatiles recycling within the lithosphere. This approach is even more important in active or dormant volcanic areas, where the signature of the gaseous emissions at the surface can be compared to that of the underlying lithospheric mantle domains. The ultramafic xenoliths brought to the surface in West Eifel (~0.5-0.01 Ma) and Siebengebirge (~30-6 Ma) volcanic fields (Germany) are ideal targets, as they can be representative of the SCLM beneath the Central European Volcanic Province. Five distinct populations from these localities were investigated by means of petrographic observations, mineral phase analyses and determination of He, Ne, Ar and CO_2 contents in olivine-, orthopyroxene- and clinopyroxene-hosted FI. Siebengebirge rocks have mostly refractory composition, made by highly forsteritic olivine, high-Mg# and low-Al pyroxene, as well as by spinel with high Cr#, reflecting high extents (up to 30%) of melt extraction. On the other hand, xenoliths from West Eifel are modally and compositionally heterogeneous, as testified by the large forsterite range of olivine (Fo_{83-92}), the Cr# range of spinel (0.1-0.6) and the variable Al and Ti contents of pyroxene. Equilibration temperatures vary from 880 to 1060°C in Siebengebirge, and from 900 to 1180 °C in West Eifel xenoliths, at oxygen fugacity values generally comprised between -0.5 and +1.2 $\Delta \log fO_2$ [FMQ]. In both areas, FI composition is dominated by CO_2, with clinopyroxene and most of the orthopyroxene having the highest volatile concentration, while olivine being gas-poor. The noble gases and CO_2 distribution suggests that olivine is representative of a residual mantle that experienced one or more melt extraction episodes. The $^3He/^4He$ ratio corrected for air contamination (Rc/Ra values) varies from 6.8 Ra in harzburgitic

lithotypes to 5.5 Ra in lherzolites and cumulates rocks, indicating that the original MORB-like mantle signature was progressively modified by the interaction with crustal-related components having the $^{3}He/^{4}He$ and $^{4}He/^{40}Ar^{*}$ values consistent with those measured in magmatic gaseous emissions. The systematics of Ne and Ar isotopes indicate that most of the data are consistent with mixing between recycled air and a MORB-like mantle, excluding the presence of a lower mantle plume beneath the Central European Volcanic Province. The major element distribution in mineral phases from West Eifel and Siebengebirge, together with the systematic variations in FI composition, the positive correlation between Al-enrichment in pyroxene and equilibration temperatures, and the concomitant Rc/Ra decrease at increasing temperature, suggest that the SCLM beneath Siebengebirge represented the German lithosphere prior to the massive infiltration of melts/fluids belonging to the Quaternary Eifel volcanism. On the other hand, West Eifel xenoliths bear witness of multiple heterogeneous metasomatism/refertilization events that took place in the German SCLM between ~6 and ~0.5 Ma.

Keywords: Eifel, Siebengebirge, Noble gases, CO_2, Fluid inclusions, Mantle xenoliths, European SCLM, Partial melting, Metasomatism, Refertilization

1. Introduction

The integrated study of petrography, mineral chemistry, and fluid inclusions (FI) composition (He, Ne, Ar, CO_2) in ultramafic xenoliths is a powerful tool for constraining the chemical features and evolution of the Sub-Continental Lithospheric Mantle (SCLM), as it is crucial for identifying the melt extraction and enrichment episodes that modified its original composition through time. Furthermore, the possibility to compare the geochemical fingerprint of mantle rocks with that of fluids rising through the crust and used for volcanic or seismic monitoring opens new perspectives on a better comprehension of the genetic causes of present natural phenomena. The intensive mobilization of fluids and volatiles from the mantle during major rifting events is testified by the emission of gases (e.g., Bräuer et al., 2013; Hilton et al., 1998; Weinlich et al., 1999), the production of alkali- and volatiles-rich melts (e.g., Bailey, 1978; Casetta et al., 2020, 2019; Foley and Fischer, 2017; Giacomoni et al., 2020; Oppenheimer et al., 2011) as well as by the melt/fluid-rock reactions recorded by ultramafic xenoliths (e.g., Aulbach et al., 2020; Rizzo et al., 2018; Shaw et al., 2018). In this respect, the volcanic areas of Eifel and Siebengebirge in Germany represent a great opportunity to test this scientific approach for three main reasons. First, these volcanic centres developed in the core of the Central European Volcanic Province (CEVP), regarding which an open debate on whether the continental rift was triggered by the presence of a plume is ongoing (Keyser et al., 2002; Ritter, 2007 and references therein; Ritter et al., 2001). Second, the occurrence of mantle xenoliths in both Siebengebirge and Eifel, together with the large age interval covered by the two magmatic provinces (from 30-6 to 0.5-0.01 Ma, respectively) provides a unique occasion for tracing the temporal evolution of the underlying SCLM. Third, the Eifel area is characterized by the presence of CO_2-dominated gas emissions and weak earthquakes, testifying that magmatic activity is nowadays dormant, but not ended (e.g., Aeschbach-Hertig et al., 1996; Bräuer et al., 2013, 2005; Giggenbach et al., 1991; Griesshaber et al., 1992; Schmincke, 2007), giving more support to constrain the behaviour of noble gas emissions in prevision of future magmatic unrests.

In the present study, we present detailed petrographic observations and mineral phase major elements chemistry coupled with measurement of noble gases and CO_2 composition of FI in olivine, orthopyroxene (Opx) and clinopyroxene (Cpx) from West Eifel and Siebengebirge ultramafic xenoliths. These data enabled us to: i) deepen the knowledge of the compositional features of the mantle beneath West Eifel, in the light of a comparison with the much less known ultramafic xenoliths from the Siebengebirge volcanic field; ii) integrate previous studies focused on the composition of FI in olivine from West Eifel (Gautheron et al., 2005) with new data from pyroxene as well as from the Siebengebirge xenoliths (Willmeroth and Eulenberg), which, as far as authors know are presented for the first time; iii) model the succession of melt extraction and enrichment (metasomatism vs. refertilization) processes recorded by xenoliths from the two volcanic fields; iv) model the thermal state of the lithospheric column and its relationships with mantle processes and magmatism; and, ultimately, v) discuss the evolution of the Cenozoic SCLM beneath Germany.

2. The Central European Volcanic Province in Germany: state of the art

2.1. Cenozoic magmatism and geodynamic framework

The German volcanic fields are part of the CEVP, which results from the development of Tertiary to Quaternary intra-continental rifts (Dèzes et al., 2004; Lustrino and Wilson, 2007; Wilson and Downes, 2006, 1991) (Fig. 1a). The most relevant volcanic areas, from W to E are: Hocheifel (~45-24 Ma) and Eifel (~0.5-0.01 Ma), Siebengebirge (~30-6 Ma), Westerwald (~32-0.4 Ma), Vogelsberg (~21-9 Ma), Hessian Depression (~21-8 Ma), Rhön (~26-11 Ma), Heldburg (~42-11 Ma) and Upper Palatinate (∼29-19 Ma) (Fig. 1b; ages from Lippolt, 1983). During Tertiary, the main volcanic manifestations occurred in the westernmost Hocheifel (Fig. 1a) and in the Siebengebirge (Fig. 1b) areas, this latter developed in association with the middle and upper Rhine rift system. The Siebengebirge volcanic field formed during Eocene to Oligocene as syn- to post-Alpine extension (Ziegler, 1992). Indeed, mafic magmas with variable degrees of SiO_2-undersaturation were erupted from ~30 Ma to 6 Ma (Frechen and Vieten, 1970a, 1970b; Kolb et al., 2012; Todt and Lippolt, 1980; Vieten et al., 1988). The Hocheifel lavas mostly intruded weakly metamorphosed Devonian and Carboniferous sediments of the Hercynian Rhenish Massif (e.g., Ernst and Bohatý, 2009). In the Quaternary, the volcanism developed in the Eifel volcanic fields in the West of the Rhine, overlapping the Hocheifel province and inducing the uplift of the Rhenish Massif since 0.8 Ma; the last known eruption at Eifel is dated 11 ka from the Ulmer Maar in the West Eifel (Zolitschka et al., 1995). Eifel volcanism comprises 250 eruptive centres over an area of 600 km^2 and is subdivided into two distinct volcanic fields, namely West and East Eifel. Each domain was developed on both sides of the maximum uplift zone. The West Eifel volcanoes sit atop the highest parts of the Rhenish Massif and started erupting less than 700 ka ago, while the lavas of the East Eifel were erupted in the Neuwied Basin since about 460 ka ago (Schmincke, 2007). In each area, the early eruptions are characterized by the emission of potassic basanites, followed by more evolved and sodic lavas (Mertes and Schmincke, 1985). Volcanoes are mainly cinder and tuff cones and maars with tuff rings whose formation is partially governed by magma-water interaction, resulting in phreatomagmatic eruptions. The West Eifel field shows a clear NW-SE trend in both the distribution of volcanoes and age of volcanism (Schmincke et al., 1983), the oldest activity belonging to the Ormont area, while the youngest to the SE sector. The frequency of volcanic eruptions has decreased during the last 100 ky (Nowell et al., 2006). Tomography studies indicate abnormal seismic velocities between 50-60 km and 410-660 km depth, interpreted as evidences of a narrow thermal plume in the asthenosphere below the Eifel (Keyser et al., 2002; Ritter, 2007; Ritter et al., 2001). On the other hand, geochemical, petrological and geodynamic studies rule out this hypothesis and propose alternative models to explain the magmatism, such as passive upwelling of the asthenosphere or crustal extension and melting of the lithospheric mantle (e.g., Lustrino and Carminati, 2007), making Eifel and the whole CEVP extremely interesting study areas.

2.2. Existing background on mantle xenoliths in West Eifel and Siebengebirge areas

West Eifel mantle xenoliths are among the most studied in the world since early 1960's. Pioneering works on Dreiser Weiher xenoliths (dunites, harzburgites, lherzolites and wehrlites) enabled to discriminate between a group of anhydrous samples equilibrated at high T, with LREE-depleted to slightly -enriched Cpx, and another made by strongly LREE-enriched rocks bearing amphibole and/or reaction textures interpreted as its breakdown, equilibrated at lower T (Stosch and Seck, 1980). To explain the misfit between the composition of anhydrous xenoliths and the simple partial melting models developed from the most fertile lherzolite, the authors suggested that Dreiser Weiher rocks record the multistage evolution, made by depletion and enrichment events, of the upper mantle beneath West Eifel at least since 2 Ga (Stosch and Lugmair, 1986). A later metasomatic episode, possibly triggered by a fluid or melt agent, was responsible for the further LREE-enrichment in Cpx, the formation of amphibole (Stosch and Seck, 1980) and the occasional co-precipitation of phlogopite (Stosch and Lugmair, 1986). Although the hypothesized model was not able to account for the genesis of the entire spectrum of lithotypes observed in West Eifel, it represented the baseline for the subsequent studies. Based on O isotopes, Kempton et al. (1988) inferred that the genesis of amphibole and phlogopite in Dreiser Weiher and Meerfelder Maar xenoliths occurred during two distinct metasomatic events. Furthermore, they suggested that the aqueous fluids responsible for the formation of hydrous phases and the general LREE-enrichment derived from recycling of crustal material introduced into the upper mantle via subduction. By means of the study of ultramafic xenoliths from Gees, Lloyd et al. (1991) identified a metasomatic/refertilization process that transformed the anhydrous harzburgites into lherzolites via interaction with a Ca-alkali-rich silicate melt. They also related the formation of phlogopite-bearing wehrlites to the infiltration of Ti-Al-Ca-K-rich hydrous melts, possibly occurring in concomitance with the young uplift of the Rhenish Shield, related to the mantle diapirism (Witt and Seck, 1987). Witt and Seck (1989) recognized different textural/compositional amphibole types in the protogranular and recrystallized mantle xenoliths: i) low-TiO_2 disseminated amphiboles, generated by small proportions of intergranular trapped fluid during the ascent of a mantle diapir; ii) high TiO_2-amphiboles, found within and near phlogopite-bearing hornblenditic veins, generated during the more recent interaction between the host peridotite and a melt similar in trace element and isotopic composition to the Quaternary West Eifel lavas (see also Witt-Eickschen et al., 1998). According to their model, the percolation of this latter melt occurred through fractures, and the interaction with the host peridotites was short-lived and localized, not being able to erase the imprint of the previous metasomatic events. Contemporarily, primitive magmas genetically linked to the Quaternary magmatism were responsible for the formation of cumulate olivine-clinopyroxenites (Witt-Eickschen and Kramm, 1998). To explain the variable trace element distribution and Sr-Nd-Pb systematics of Cpx and amphibole in xenoliths from several West Eifel localities, Witt-Eickschen et al. (2003) and Witt-Eickschen (2007) hypothesized the occurrence of three distinct metasomatic episodes. The first event caused the formation of disseminated amphibole during deformation in the shallow SCLM, in concomitance with the infiltration of isotopically-enriched (EM-like) aqueous fluids related to the ancient Hercynian subduction. During a second episode, the enriched SCLM was metasomatized by melts derived from a HIMU-like mantle component, probably in concomitance with the Cretaceous nephelinitic magmatism in the Eifel area. In this context, the HIMU-like signature was related to the reactivation of ancient subducted crustal domains (Witt-Eickschen, 2007). The third episode was the veining of the shallow SCLM linked to the Cenozoic Eifel magmatism. As an alternative, the same authors proposed that the compositional heterogeneities recorded in the peridotites were not linked to temporally distinct episodes, being instead caused by the infiltration of metasomatic melts deriving from different, heterogeneous mantle domains (Witt-Eickschen et al., 2003). The subsequent detailed work by Shaw et al. (2005) brought the investigation perspective from regional to local, highlighting that the compositional differences between magmas erupted at Dreiser Weiher, Meerfelder Maar and those emitted at Gees, Baarley and Rockeskyller Kopf are accompanied by textural, modal and compositional differences between the corresponding entrained xenoliths. On the other hand, they noticed that during each metasomatic event, the composition, fluid content and flow rate/flux of the melt, the permeability and reactivity of the host peridotite and the duration of the melt/rock interaction may have varied drastically even upon short distances, causing strong heterogeneities in the SCLM. Numerical simulations, for example, showed that the origin of phlogopite-bearing wehrlites from Rockeskyller Kopf could be modelled via a reaction between harzburgites/lherzolites and undersaturated, K-rich alkaline melts similar to magmas emitted in the volcanic field (Shaw et al., 2018). Although showing small discrepancies between real and calculated products - likely ascribable to variable equilibration times of olivine and Cpx and the variable degrees of actual equilibration between the initial phases and those formed during the reaction with the melt at the time of the rapid transport of the xenoliths to the surface (Shaw et al., 2018) - such a model corroborated the view about the complexity of the metasomatism experienced by the Eifel SCLM.

Contrary to Eifel occurrences, mantle xenoliths from Siebengebirge volcanic field are little known. Moreva-Perekalina (1985) firstly described in detail the highly variable petrographic features of ultramafic enclaves in alkali-basalts from Finkenberg. The samples span from spinel-bearing, anhydrous lherzolites and harzburgites to websterites and phlogopite±amphibole-bearing wehrlites and clinopyroxenites. The phlogopite in the latter may be found as disseminated crystals and/or veins; apatite and carbonate could be present as accessory phases. Witt and Seck (1989) reported some information about Siebengebirge peridotites in a regional overview on the SCLM beneath the Rhenish Massif, but avoided to put forward a comparison between single localities and/or between them and the xenoliths suites brought to the surface by the younger magmatic episodes in the Eifel area.

3. Sampling and analytical methods

3.1. Sample location and preparation

Ultramafic xenoliths were sampled in West Eifel (Meerfelder Maar, Gees, Dreiser Weiher) and Siebengebirge (Eulenberg, Willmeroth) volcanic centres (Fig. 1c). Most of the xenoliths were hosted within lava, sills and/or necks (Siebengebirge) (Fig. 1d-1e), as well as within scoria cone and/or pyroclastic deposits (West Eifel) (Fig. 1f), and were sampled in active quarries or in fresh surface within maars or compact lavas. The xenoliths are typically 5-15 cm in diameter (occasionally up to 20 cm) and are relatively abundant in some locations from West Eifel (e.g., Meerfelder Maar and Dreiser Weiher). The largest and less altered samples were cut, sliced, and polished into 80-μm-thick sections for defining the modal composition, petrography, and mineral chemistry. Based on xenoliths dimensions and the feasibility of hand-picking hundreds of milligrams of crystals, 46 aliquots of pure and unaltered olivine (n=18), Opx (n=17), and Cpx (n=11) were separated for measuring the noble gases and CO_2 in FI. After samples grinding and sieving, crystals without impurities and larger than 0.5 mm were handpicked following the lab protocol developed at the Istituto Nazionale di Geofisica e Vulcanologia (INGV), Sezione di Palermo, Italy (Rizzo et al., 2018 and references therein). Mineral aliquots were then cleaned ultrasonically in 6.5% HNO_3 for noble gases and in 6.5% HCl for CO_2 measurements, before being rinsed with deionized water and acetone in an ultrasonic bath. Around 0.10-0.85 g of sample were loaded into the crusher for analyses.

3.2. Mineral chemistry analyses

Mineral phase major element chemistry was determined by using a Cameca SXFive FE electron microprobe equipped with five WD and one ED spectrometers hosted in the Department of Lithospheric Research at the University of Wien. The operating conditions were as follows: 15 kV accelerating voltage, 20 nA beam current, and 20 s counting time on peak position. Natural and synthetic standards were used for calibration, and PAP corrections were applied to the intensity data (Pouchou and Pichoir, 1991).

3.3. Noble gases and CO_2 measurements in fluid inclusions

Element and isotope composition of noble gases (He, Ne, and Ar) and CO_2 concentration in FI was determined at the Noble gas isotope laboratory of INGV-Palermo in Italy. The selected crystals were loaded into a stainless-steel crusher capable of holding up to six samples simultaneously for noble-gas analysis. FI were released by in-vacuo single-step crushing of minerals at about 200 bar applied by a hydraulic press. This conservative procedure was used to minimize the contribution of cosmogenic ^3He and radiogenic ^4He that could possibly have grown or been trapped in the crystal lattice (Hilton et al., 2002, 1993; Kurz, 1986; Rizzo et al., 2018, 2015). However, since our samples were collected in a quarry, and have been shielded from cosmic rays for most of their history, there should have been no cosmogenic effect. The CO_2 estimation was first performed during noble-gas extraction at the time of crushing by quantifying the total gas pressure (CO_2+N_2+O_2+noble gases) and subtracting the residual pressure of N_2+O_2+noble gases after removing CO_2 using a “cold finger” immersed in liquid N_2 at –196°C. The noble gases were then cleaned under getters in an ultra-high-vacuum (10^{-9}–10^{-10} mbar) purification line, and all species in the gas mixture except for noble gases were removed. A cold finger with active charcoal immersed in liquid N_2 then removed Ar, while He and Ne were separated by using a cold head cooled at 10°K and then moved at 40 and 80°K in order to release He and Ne, respectively.

He isotopes (^3He and ^4He) and Ne isotopes (^{20}Ne, ^{21}Ne, and ^{22}Ne) were measured separately using two different split-flight-tube mass spectrometers (Helix SFT, Thermo Scientific). The values of the $^3He/^4He$ ratio are expressed in units of R/Ra, where Ra is the $^3He/^4He$ ratio of air, which is equal to 1.39×10^{-6}. The analytical uncertainty for the He-isotope ratio (1σ) was generally <10% except for a few gas-poor samples, while for $^{20}Ne/^{22}Ne$ and $^{21}Ne/^{22}Ne$ this was generally <5% and <10%, respectively. The reported values of both Ne-isotope ratios are corrected for isobaric interferences at m/z values of 20 ($^{40}Ar^{2+}$) and 22 ($^{44}CO_2^{2+}$). Corrections are generally performed by measuring ^{20}Ne, ^{21}Ne, ^{22}Ne, ^{40}Ar, and $^{44}CO_2$ during the same analysis, and considering the previously determined $^{40}Ar^{2+}/^{40}Ar^+$ and $^{44}CO_2^{2+}/CO_2^+$ ratios on the same Helix SFT that run FI samples. Ar isotopes (^{36}Ar, ^{38}Ar, and ^{40}Ar) were analysed by a multi-collector mass spectrometer (Argus, GVI) with an analytical uncertainty (1σ) of <1.0%. To quantify the concentration and isotope ratios of He, Ne and Ar, we used an air standard that had previously been purified from the atmosphere and stored in separate tanks. The analytical uncertainty (1σ) values for the $^3He/^4He$, $^{20}Ne/^{22}Ne$, $^{21}Ne/^{22}Ne$, $^{40}Ar/^{36}Ar$, and $^{38}Ar/^{36}Ar$ ratios were <0.94%, <0.07%, <0.3%, <0.05%, and <0.12%, respectively. These values represent the standard deviation of measurements made during>1 year of analyses for He and Ne and 2 years for Ar. The uncertainty in the determinations of the elemental He, Ne, and Ar contents was <0.1%; typical blanks for He, Ne, and Ar were $<10^{-15}$, $<10^{-16}$, and $<10^{-14}$ mol, respectively. Further details about the sample preparation and analytical procedures are available in Rizzo et al. (2018) and Faccini et al. (2020). Although most of the samples showed a low atmospheric contamination (air has $^4He/^{20}Ne = 0.318$, $^{20}Ne/^{22}Ne = 9.8$, $^{21}Ne/^{22}Ne = 0.029$, and $^{40}Ar/^{36}Ar = 295.5$; Ozima and Podosek, 2002), $^3He/^4He$ was corrected for contamination based on the measured $^4He/^{20}Ne$ ratio as follows:

$$Rc/Ra = ((R_M/Ra)(He/Ne)_M - (He/Ne)_A)/((He/Ne)_M - (He/Ne)_A)$$

where subscripts M and A refer to measured and atmospheric theoretical values, respectively. The corrected $^3He/^4He$ ratios are hereafter reported as Rc/Ra values. However, the correction was either small or negligible for most of the samples. ^{40}Ar was corrected for air contamination ($^{40}Ar^*$) assuming that the measured ^{36}Ar was entirely of atmospheric origin as follows:

$$^{40}Ar^* = {}^{40}Ar_{sample} - [{}^{36}Ar_{sample} \times ({}^{40}Ar/{}^{36}Ar)_{air}]$$

$$^{40}Ar_{air} = {}^{40}Ar_{sample} - {}^{40}Ar$$

4. Results

4.1 Petrography

In the following lines, a summary of the main petrographic features of West Eifel and Siebengebirge samples is reported. For a more exhaustive description, see Supplementary Material File 1.

4.1.1 West Eifel ultramafic xenoliths

Ultramafic enclaves from West Eifel include a large variety of rock types and textures, resembling what already reported in the literature (see Witt-Eickschen, 2007 and references therein). Meerfelder Maar mantle xenoliths include five anhydrous, two amphibole-bearing and one phlogopite-amphibole bearing lherzolites, one amphibole-bearing harzburgite and one phlogopite-bearing wehrlite (Table 1; Figg. 2 and S1). Half of the samples have coarse- to medium-grained textures that vary between pure to slightly foliated protogranular types (Mercier and Nicolas, 1975). The remaining are transitional between protogranular and mosaic equigranular (Mercier and Nicolas, 1975) or pure mosaic equigranular. Amphibole is found in three types of textures. In the first case, it is present in the protogranular samples as small, well-equilibrated tabular crystals associated to Cpx and/or spinel; this kind of amphibole grains are also observed in the proximity of an infiltrating melt vein, attached to matrix Cpx. The second textural type, found only in MM3, refers to amphibole growing within the melt vein, associated with secondary Cpx. The third type can be found in the protogranular-equigranular samples: amphibole (±phlogopite) has a mosaic shape and it often shows reaction rims, where glass and tiny subhedral to euhedral secondary phases (mainly Cpx, olivine and spinel) are present. Additionally, in some of the equigranular areas, glass pools occupies the textural position of a previous phase (probably Cpx and/or amphibole), together with tiny subhedral to euhedral secondary phases (olivine, Cpx and opaques). In MM1, strongly pleochroic phlogopite can be found either in association with infiltrating veinlets from the host basalt or texturally equilibrated, close to spinels.

Dreiser Weiher xenoliths (Table 1; Figg. 2 and S1) include five anhydrous lherzolites, one anhydrous harzburgite, one anhydrous wehrlite, one amphibole-phlogopite-bearing wehrlite, one olivine-clinopyroxenite and two anhydrous composite xenoliths: a lherzolite/olivine-clinopyroxenite (DBR1 Pd + DBR1 Px) and a lherzolite crosscut by a dunite channel (DBR10 Pd + DBR10 Dn). Lherzolites share a medium-grained protogranular texture, with spinel present as blobs and/or vermicular crystals. The harzburgite has mosaic equigranular features, where glass occurs in a texture similar to that already described for Meerfelder Maar equigranular samples. DBR2 is a coarse-grained, recrystallized cumulate; wehrlite DBR4 has tabular equigranular texture partially disrupted by a massive melt infiltration, with amphibole and phlogopite texturally equilibrated with Cpx and olivine in the preserved areas. DBR1 Px and DBR11 are medium to very coarse-grained olivine-clinopyroxenites with orthocumulitic texture. The contact between DBR1 Px and the lherzolitic portion is gradual and can be identified by a wehrlitic band, where Cpx is similar to those of the olivine-clinopyroxenite and rich in fluid inclusions. Composite sample DBR10 consists of a medium-fine-grained protogranular lherzolite cut by a spinel-rich dunitic channel.

Gees samples includes three anhydrous harzburgites, one anhydrous lherzolite, one anhydrous olivine-websterite, one anhydrous olivine-clinopyroxenite, and four phlogopite-bearing wehrlites (Table 1; Figg. 2 and S1). The harzburgites and the lherzolite are characterized by porphyroclastic texture, with Opx as the largest porphyroclasts. Opx and spinel are often characterized by a reaction rim composed of glass and secondary Cpx. This feature has been related to wehrlitization processes (Aulbach et al., 2020; Shaw et al., 2005) however, also the few primary Cpx relics are completely spongy. The wehrlites and the olivine-clinopyroxenite basically consist of previous ad-cumulitic textured dunites, subsequently infiltrated at various degrees by an incoming melt. The primary olivine are coarse-grained and highly inequigranular, often fractured. Sub-idiomorphic secondary olivine, sub-idiomorphic to allotriomorphic green Cpx, rounded spinel and phlogopite (if present) have crystallized from the infiltrating melt in pockets and large clusters between and/or around the primary olivine grains. The phases appear well equilibrated in most cases although some Cpx have spongy rim, especially when surrounded by, or near to, glass veinlets and pools. In GE8, a sub-millimetric phlogopite-bearing vein cut the sample. Olivine-websterite GE1 has texture grading from adcumulitic, composed of coarse-grained Opx and Cpx, to orthocumulitic, with olivine crystals as backbone and smaller pyroxene + spinel as intercumulus phases. Cpx destabilization is widespread, visible as spongy surfaces, composed by secondary phases surrounded by a glass film.

4.1.2 Siebengebirge ultramafic xenoliths

Siebengebirge anhydrous, spinel-bearing ultramafic xenoliths were sampled from two localities: a quarry near to Willmeroth village and the Eulenberg neck. Low-T alteration is present in both xenoliths suites, being more developed than in West Eifel rocks. Willmeroth xenoliths are mainly harzburgites with subordinated dunites and only one lherzolite (Table 1; Figg. 2 and S1). The harzburgites and lherzolite have coarse-grained porphyroclastic texture, where Opx is present only as porphyroclasts with well-developed exolution lamellae. It always shows a reaction texture characterized by spongy, recrystallized rims of Cpx, whose aggregates often extends to engulf the spinels. Primary Cpx is also completely spongy or cribrose. Dunites have texture varying from mildly porphyroclastic to mosaic equigranular tending towards II generation protogranular (Mercier and Nicolas, 1975). Spinel is rounded and generally arranged in aligned clusters. Secondary green Cpx is abundant throughout the dunite matrix, often present around the spinels and/or immersed in an altered glassy matrix together with plagioclase and opaques.

Eulenberg mantle xenoliths are all porphyroclastic harzburgites and are very similar to Willmeroth harzburgites (Table 1; Figg. 2 and S1), except for some small, better preserved, primary Cpx cores showing well-developed exsolution lamellae.

5. Mineral chemistry

5.1. Olivine

Olivine in West Eifel ultramafic xenoliths is characterized by a large compositional variations (Table S1), testifying for the occurrence of both typical mantle lithologies (harzburgites and lherzolites), reaction products, and cumulates (Herzberg et al., 2016). Its forsterite (Fo) content varies from 83.4 to 91.6, while NiO spans between 0.16 to 0.42 wt% (Fig. 3). On the other hand, olivine in Siebengebirge xenoliths have Fo and NiO contents varying from 90.5 to 91.8 and from 0.31 to 0.43, respectively.

5.2. Clinopyroxene

Cpx in West Eifel ultramafic xenoliths have a very large compositional spectrum, with Mg# and Al_2O_3 varying from 84.4 to 92.6 and from 2.22 to 8.65 wt%, respectively (Table S2; Fig. 4a). Cpx in both lherzolites and harzburgites (Mg# ≥88.7) and in other ultramafic parageneses (Mg# < 88.7) may reach both low and high Al_2O_3 contents, lying onto well-defined trends with different Mg#/Al_2O_3 ratios (see also Coltorti et al., 2020; Melchiorre et al., 2020). Cpx in West Eifel xenoliths are generally characterized by increasing TiO_2

content with decreasing Mg#, except for the olivine-websterite, where Cpx has remarkably low TiO_2 (Fig. 4b).

Among Siebengebirge xenoliths, Cpx has often secondary origin (e.g. in Willmeroth samples), but remnants of primary phases can be also found, as in case of Eulenberg rocks. In the first case, Cpx has Mg# spanning from 88.6 to 94.1 and Al_2O_3 from 0.66 to 5.10 wt% (Table S2; Fig. 4a), while in the second it results more compositionally homogeneous (Mg# 91.6-94.1; Al_2O_3 1.43-3.98 wt%). Remarkably, the TiO_2 content in Willmeroth secondary Cpx increases up to 1.21 wt%, while in Eulenberg phases it is very low (≤0.22 wt%) (Fig. 4b), as expected for a restitic assemblage.

5.3. Orthopyroxene

Opx composition in West Eifel xenoliths is rather constant within each sample. The Mg# ranges from 84.4-85.2 in the olivine-websterites to 89.0-92.2 in the lherzolites and harzburgites (Table S3; Fig. 4c), and is accompanied by large Al_2O_3 variations (1.47-6.47 wt%, Fig. 4c). TiO_2 is usually low (≤0.15 wt%) for the majority of Opx (Fig. 4d), whereas it reaches higher values (up to 0.30 wt%) in the most fertile assemblages. Opx in Siebengebirge rocks is more depleted than in West Eifel ones, with a partial overlap of both Mg# (90.6-92.0) and Al_2O_3 (≤3.36 wt%) ranges (Table S3; Fig. 4c). TiO_2 content is also generally low (≤0.23 wt%, Fig. 4d).

5.4. Spinel

Spinel in West Eifel ultramafic xenoliths has Mg# and Cr# varying from 40.8 to 77.5 and from 9.54 to 57.2, respectively (Table S4). The lower Mg# values belong to spinel in the olivine-websterite from Gees. Spinel in Siebengebirge xenoliths has similar Mg# with respect to West Eifel rocks (49.6-77.3), but higher Cr# (15.8 to 81.7) (Table S4). Willmeroth spinel has bimodal composition, with a Cr-rich group and an Al-rich group, as can be easily noticed in the Olivine-Spinel Mantle Array (OSMA) diagram of Figure 5.

6. Redox and thermal state of the SCLM beneath Germany

Equilibration temperatures of West Eifel and Siebengebirge xenoliths were calculated by means of the olivine-spinel exchange thermometer of Ballhaus et al. (1991), at an assumed pressure of 1.5 GPa, which is roughly the centre of the pressure range for spinel stability. We used compositions obtained from the cores as well as from the rims of grains, which were homogeneous within a given grain. Temperatures for our xenoliths are averages determined from multiple olivine-spinel pairs. Differences in calculated T are small and have negligible influences on the results of oxybarometric computations which, furthermore, are referenced to the FMQ buffer to minimize the effects of T uncertainties (see below). Calculated T vary between 880 °C in harzburgites from both localities and 1180 °C in anhydrous lherzolites from West Eifel

(Table 1). In general, the equilibration T recorded by West Eifel amphibole- (± phlogopite) bearing rocks lie in a narrow range, comprised between ~950 and ~1050 °C, while anhydrous xenoliths from the same locality reach the highest T conditions, confirming what already noticed by Stosch and Seck (1980) and Witt-Eickschen (2007). On the other hand, the absence of temperature gaps between anhydrous and amphibole-bearing xenoliths and the T overlap between Siebengebirge and West Eifel rocks lead to exclude a systematic modal/compositional zoning of the German SCLM.

The oxygen fugacity recorded by spinel peridotites can be determined by using any of the calibrated heterogeneous chemical equilibria (e.g., $2\ Fe_3O_4 + 3\ Fe_2Si_2O_6 = 6\ Fe_2SiO_4 + O_2$ or $2\ Fe_3O_4 + 3SiO_2 = 3\ Fe_2SiO_4 + O_2$), with the most sensitive compositional parameter of fO_2 being the spinel ferric/ferrous iron ratio. The Fe^{3+} content of spinels from our xenoliths was calculated from microprobe analysis assuming perfect stoichiometry; comparison of stoichiometric vs. Mössbauer spectroscopy $Fe^{3+}/\sum Fe$ ratios in spinels indicates that this method yields reasonable results (e.g., Canil and O'Neill, 1996). Oxygen fugacity was calculated relative to the FMQ buffer based on the olivine-spinel-Opx oxygen barometer of Miller et al. (2016). This formulation was selected because it has the strong advantage of solving several reactions simultaneously by the least-squares method, providing a solid fO_2 estimate within an accuracy of about ±0.3 to 0.6 log units. For comparison, fO_2 was also calculated with older calibrations available in the literature (e.g., Ballhaus et al., 1991; Bryndzia and Wood, 1990), yielding similar results (Table 1). Just as for temperatures, $\Delta \log fO_2$ [FMQ] for our xenoliths are averages determined from multiple olivine-spinel-Opx sets. Differences in calculated fO_2 are generally small, suggesting redox equilibrium; only two samples (SB2 and SB6) yielded significant variations in fO_2, comparable to the accuracy of the method. Calculated $\Delta \log fO_2$ [FMQ] values (Table 1) vary between ca. -0.5 and +1.2, with most of the data lying at $\Delta FMQ > 0$ (Fig. 6). Taken collectively, Siebengebirge samples (bulk refractory compositions, mainly harzburgites) record lower temperatures than those from the West Eifel domain (more fertile compositions, mainly lherzolites). Systematics in fO_2 are less marked, but Siebengebirge samples tend to be generally more oxidized (except for SB2 and SB6 samples, which record distinctly negative $\Delta \log fO_2$ [FMQ] values) than those from the West Eifel domain (Fig. 6).

7. Occurrence and chemistry of FI

7.1. Description of FI

The dimension, occurrence and typology of FI in West Eifel and Siebengebirge samples were assessed by optical microscopy observation on thin sections. In both xenolith populations, FI are quite numerous in both olivine, Opx and Cpx, especially in association with the occurrence of intergranular reaction zones, to which FI are sometimes related. The size of FI is heterogeneous, as their diameter ranges from few µm to tens of µm (Fig. S2). Usually, isolated FI are larger than those arranged in trails. In accordance with what already observed by Gautheron et al. (2005) and Rizzo et al. (2018), two main FI genetic types (primary vs. secondary) were identified among West Eifel and Siebengebirge xenoliths, following the classification of Roedder (1984). The first type encompasses the isolated inclusions found within single grains, as well as FI clusters and/or trails crossing specific crystals but being unconnected to the neighbouring phases or to the reaction zones (Fig. S2). This type is the most abundant in both xenolith populations, and typical of mantle lithologies. The second type comprises inclusions aligned within exsolution lamellae in Opx and Cpx, and clusters/trails of FI propagating through neighbouring phases (Fig. S2). This type of FI, rarer and found mostly in cumulates, is prone to be entrapped during recrystallization events, and is usually accompanied by the occurrence of evident reaction zones at the crystal edges or along veins, which bear witness of post-melt extraction enrichment processes.

7.2. Chemistry of FI

The chemistry of FI hosted in West Eifel and Siebengebirge xenoliths is reported in Table S5 and shown in Figure 7. $^{40}Ar^*$ is within the range of 0.3–65.7×10^{-12} mol/g, while ^{4}He ranges from 0.1×10^{-12} to 40.8×10^{-12} mol/g (Fig. 7a) and ^{3}He from 0.7×10^{-18} to 330×10^{-18} mol/g (Table S5). The gas mixture is dominated by CO_2, which spans in a wide range from 2.5×10^{-11} to 1.3×10^{-6} mol/g (Fig. 7b). N_2 corrected for atmospheric contamination (N_2^*) represents the second major species, whose content varies from 0.09×10^{-9} to 11.1×10^{-9} mol/g (Fig. 7c). The atmospheric component in FI, which here is considered to be N_2+O_2+Ar, varies from 1.5×10^{-11} to 87.1×10^{-11} mol/g. The ^{20}Ne concentration ranges from 0.4×10^{-15} to 68.5×10^{-15} mol/g (Table S5). Finally, $^{21}Ne^*$ varies from 0.6×10^{-19} to 81×10^{-19} mol/g (Fig. 7d).

The average numbers of mol/g of CO_2, N_2^*, $^{40}Ar^*$, $^{21}Ne^*$, and ^{4}He are higher in Cpx and Opx than in olivine. In addition, samples from West Eifel are gas richer than those from Siebengebirge (Fig. 7), generally reflecting the same proportions among mineral phases above reported. Due to the extremely depleted lithology, it was not possible to make measurements in Cpx from Siebengebirge. CO_2 is positively correlated with N_2^*, $^{40}Ar^*$, $^{21}Ne^*$, and ^{4}He, indicating that the CO_2-rich FI are also rich in the other gas species.

The $^{3}He/^{4}He$ ratio not corrected for air contamination (R/Ra) is 5.5-6.8 Ra in olivine, 3.1-6.8 Ra in Opx, and 5.6-6.8 Ra in Cpx (Table S5). The $^{4}He/^{20}Ne$ ratio is 182-1761 in olivine, 20-2754 in Opx, and 596-4929 in Cpx (Table S5). The $^{40}Ar/^{36}Ar$ ratio is 345-2344 in olivine, 328-7192 in Opx, and 1170-9797 in Cpx (Table S5). The $^{20}Ne/^{22}Ne$ and $^{21}Ne/^{22}Ne$ ratios are 9.8-11.0 and 0.0288-0.04372, respectively, in olivine, 9.8-10.9 and 0.0290-0.0386 in Opx, and 9.8-11.0 and 0.0298-0.0417 in Cpx (Table S5).

The $^{3}He/^{4}He$ ratio corrected for air contamination (Rc/Ra values) is 5.5-6.8 Ra in olivine, 3.1-6.8 Ra in Opx, and 5.6-6.8 Ra in Cpx (Table S5; Fig. 8). There is no systematic difference in the Rc/Ra values among variable FI concentration, different mineral phases, and regional provenance of xenoliths (West Eifel and Siebengebirge) (Fig. 8). The only exception is for Opx from SB5 that show the lowest Rc/Ra values (in 2 measurements) and also the lowest ^{4}He, ^{40}Ar* and ^{3}He content (Fig. 8). It is worth noting that samples MM1, GE1, and DBR2 (Mg# <88) show ^{3}He/^{4}He ratio progressively decreasing from 6.4 to 5.5 Ra (Table S5).

8. Discussion

8.1. Processes that could modify the geochemistry of FI

8.1.1 Atmospheric contamination

The isotopic compositions of Ne (^{20}Ne/^{22}Ne and ^{21}Ne/^{22}Ne), Ar (^{40}Ar/^{36}Ar), and ^{4}He/^{20}Ne in FI from Eifel and Siebengebirge xenoliths show variable extent of atmosphere-derived contamination, with Cpx and Opx poorly contaminated respect to olivine (Table S5). The extent of this contamination seems proportional to the concentration of gas species in FI, therefore it results that xenoliths from Siebengebirge are more contaminated respect to those from West Eifel. This is evident in the three Ne isotopes plot (Fig. 9a), in which our data fall along the theoretical air-MORB mixing line defined by Sarda et al. (1988) and Moreira et al. (1998) at ^{21}Ne/^{22}Ne = 0.06 and ^{20}Ne/^{22}Ne = 12.5. Argon isotopes coupled with He isotopes give a similar indication, as it can be observed in Fig. 9b where xenoliths from West Eifel and Siebengebirge fall along the theoretical air-MORB mixing line defined by Moreira et al. (1998) and Ballentine et al. (2005) at ^{40}Ar/^{36}Ar up to 44,000 and ^{3}He/^{36}Ar~0.45, unless their variability in ^{4}He/^{40}Ar*. Similar indications were found by Gautheron et al. (2005) for Ne and Ar isotopes in olivine from West Eifel mantle xenoliths.

If we compare xenoliths from Eifel and Siebengebirge with those from other European localities that were analyzed by single-step crushing and for which ^{40}Ar/^{36}Ar data are available, we notice that some Cpx and Opx from West Eifel show the lowest atmosphere-derived contamination, irrespective of the concentration of gas species in FI. It is worth noting that ^{40}Ar/^{36}Ar values as high as 9,797 were never been measured in mantle xenoliths from Europe and, at the best of our knowledge, from worldwide continental areas (^{40}Ar/^{36}Ar <9,060; Matsumoto et al., 2000). In fact, xenoliths from Lower Silesia are slightly more contaminated although they showed higher CO_2 and N_2* concentration, comparable ^{40}Ar* and ^{21}Ne* content but slightly lower He content than those from West Eifel (Fig. 9). Instead, xenoliths from Tallante and Calatrava (Spain, Martelli et al., 2011) as well as Persani Mts. (Transylvania, Faccini et al., 2020) show the highest contamination among the studied European localities (Correale et al., 2012; Gautheron et al., 2005; Martelli et al., 2011; Rizzo et al., 2018), which tends toward ^{40}Ar/^{36}Ar more typical of subduction-related settings (e.g., Stromboli; Martelli et al., 2014). The contamination of FI by atmosphere-derived fluids is common in SCLM xenoliths from other worldwide localities (Correale et al., 2019, 2016; Gurenko et al., 2006; Matsumoto et al., 2002, 2001, 2000, 1998; Valbracht et al., 1996; Yamamoto et al., 2004). Although it is reasonable to suppose that part of this contamination originates from post-eruptive entrapment in mineral micro-cracks (e.g., Nuccio et al., 2008) and/or during the ascent within the crust of the xenoliths-bearing magma (e.g., Gautheron et al., 2005), we argue that it represents a feature typical of SCLM mantle that was contaminated by the recycling of atmosphere-derived fluids due to active or fossil subductions (Faccini et al., 2020; Gurenko et al., 2006; Matsumoto et al., 2001, 2000, 1998; Rizzo et al., 2018; Sarda, 2004; Yamamoto et al., 2004). In addition to this recycling into the SCLM, we infer that the occurrence and superimposition to partial melting of metasomatic and refertilization processes play an additional role in defining the extent of atmosphere-derived contamination.

8.1.2 Diffusive fractionation

When plotting $^3He/^4He$ versus the concentration of ^3He and ^4He (Fig. 8), we notice that Opx from xenolith SB5 show Rc/Ra values below the range of other xenoliths (3.1-3.3 Ra versus 5.5-6.8 Ra). This behaviour is similar to what observed in SCLM xenoliths from other European localities (Faccini et al., 2020; Gautheron et al., 2005; Martelli et al., 2011) and can be appreciated at low ^3He, ^4He (Fig. 8) and $^{40}Ar^*$ concentrations, originating from preferential diffusive loss of these gases (e.g., Burnard, 2004; Burnard et al., 1998; Harrison et al., 2004; Yamamoto et al., 2009). This process depends on the diffusion coefficient (D), which is significantly higher for ^4He than for $^{40}Ar^*$ (D_{4He}/D_{40Ar} = 3.16 in solid mantle; Burnard, 2004; Yamamoto et al., 2009). In case of diffusive loss of helium, we also expect to see $^3He/^4He$ fractionation due to the appreciable difference in D_{3He} and D_{4He} among mantle minerals (D_{3He}/D_{4He} = 1.15; Burnard, 2004; Trull and Kurz, 1993; Yamamoto et al., 2009 and references therein). Faccini et al. (2020) explained the variability of the data from Persani Mts. (Transylvania) through two possible diffusive fractionation paths of ^4He, $^{40}Ar^*$, $^3He/^4He$, and $^4He/^{40}Ar^*$ during mantle melting, based on the approach of Burnard et al. (1998), Burnard (2004) and Yamamoto et al. (2009). Applying the same rationality, we can speculate that very similar boundary conditions are valid for the mantle beneath Siebengebirge, where diffusive fractionation modified the signature of Opx in SB5 harzburgite (Figg. 8 and 10). For this reason, Opx from SB5 will not be considered as representative of the mantle conditions beneath Siebengebirge area.

8.2. Partial melting of the mantle

8.2.1 Indications from mineral chemistry

The modal compositions and mineral chemistry of West Eifel and Siebengebirge mantle xenoliths can provide useful insights on the melting history experienced by the sampled lithospheric sections (Fig. 2). As shown in Figure 2b, most of the Siebengebirge xenoliths lies within the area bounded by the anhydrous melting model paths at 2 and 1 GPa (Bénard et al., 2018; Niu et al., 1997), whereas West Eifel xenoliths are best fitted by the hydrous melting paths at 1 GPa and 0.1 to 1 wt% of H_2O (Fig. 2a). According to the OSMA diagram (Fig. 5), olivine-spinel pairs in Siebengebirge xenoliths record variable melt extraction degrees, comprised between >30% (Willmeroth harzburgites) and 5-10% (Willmeroth lherzolites). Among them, a subgroup is constituted by Eulenberg harzburgites, which show a partial melting range comprised between

5 and 15%. Olivine-spinel pairs in West Eifel xenoliths, on the other hand, have more fertile composition and record less heterogeneous melt extraction degrees, comprised between 5-10% (Dreiser Weiher lherzolites) and 15-20% (Meerfelder Maar lherzolites) (Fig. 5). The distribution of Al_2O_3 and MgO in Cpx and Opx (Fig. 6b-6c) reflects the heterogeneity of the studied samples, which likely bear witness of complex melt extraction and subsequent enrichment (metasomatism/refertilization) processes. For example, Cpx in Siebengebirge harzburgites has composition varying from refractory (Mg-enriched and Al-depleted) to significantly Al-enriched, likely indicative of a secondary origin (Fig. 6b). Opx in Siebengebirge harzburgites has always refractory nature, and records melt extraction degrees as high as ~30-32% if compared to the melting trend proposed by Bonadiman and Coltorti (2011) and Upton et al. (2011) (Fig. 6c). Similar behaviour typifies Opx in harzburgites from Gees (West Eifel), which mostly record melting degrees of 22-30% (Fig. 6c). Cpx from Gees rocks lies on the same Al_2O_3-MgO trend as Cpx from Siebengebirge harzburgites (Fig. 6b). Pyroxene in the xenoliths from the other West Eifel localities (i.e. Meerfelder Maar and Dreiser Weiher) has generally more fertile composition. Opx in Meerfelder Maar amphibole- and/or phlogopite-bearing lherzolites record melt extraction degrees of 17-20% (Fig. 6c), comparable to those recorded by Opx in amphibole-phlogopite-free lherzolites (10-17%) from the same locality. Cpx in Dreiser Weiher lherzolites is enriched in Al_2O_3 with respect to that from Meerfelder Maar and Gees xenoliths, at comparable MgO contents (Fig. 6b). The same is true for Opx in Dreiser Weiher lherzolites, which results significantly Al-enriched and Mg-depleted with respect to those in other xenoliths, lying in proximity of the PM pole or even above (Fig. 6c). In general, petrographic and mineral chemical features indicate that West Eifel and Siebengebirge experienced complex and distinct partial melting histories, which seem partially masked by the superimposition of metasomatic and/or refertilization processes. In detail, Siebengebirge rocks indicate that the SCLM beneath this area experienced higher degrees of melt extraction (~15-30%) respect to West Eifel (~0-25%) (Figg. 2, 4 and 5), with minor overprinting by metasomatic process.

8.2.2 Indications from noble gases and CO_2 in fluid inclusions

The composition of FI in West Eifel and Siebengebirge xenoliths can be used to integrate the mineral chemistry-based knowledge of partial melting processes in the SCLM. If we assume that the noble gases content of FI mirrors the magnitude of melt extraction processes, then we should expect a progressive depletion in noble gases concentrations with increasing residual nature of the mantle. This reasoning assumes equal number density of fluid inclusions in all the samples, so we think that every consideration must be limited at least within each mineral phase (e.g., olivine). This is due to the noble gas incompatibility with the mineral phase, as suggested by the crystal-melt partition coefficient indicated by Heber et al. (2007). As already evidenced by Rizzo et al. (2018), caution must be paid when modelling and estimating absolute degrees of partial melting by using data from FI, because the modelling is based on crystal-melt coefficients that presuppose the partition of noble gas in the crystal lattice rather than in FI. However, Rizzo et al. (2018) noticed that in case of equilibrium between FI and crystal lattice, the variation of noble gas concentrations and ratios (e.g., $^{4}He/^{40}Ar^*$) in FI follows the expected path based on crystal-melt partition coefficients while the estimated absolute percentage of partial melting remains unrealistic. This is more evident in olivine than in Opx and Cpx, which are often subject to recrystallization during metasomatism and/or refertilization (e.g., Faccini et al., 2020; Rizzo et al., 2018).

As stated above, only a few samples from Siebengebirge and West Eifel seem to bear witness of the partial melting events, while most of them were modified by the superimposition of one or more metasomatic and/or refertilization events. Cumulate xenoliths such as MM1, GE1 and DBR2, not representative of residual mantle, are clearly identifiable by the low Mg# (<88) of the mineral phases, as well as by their $^{4}He/^{40}Ar^*$ range (0.5-4.0), more typical of magmatic values (see Section 6.6) and fertile mantle ($^{4}He/^{40}Ar^*$=1-5; Marty, 2012) (Figg. 11 and S3). The concentrations of noble gas and N_2^* in FI from the other xenoliths show a general higher depletion in samples from Siebengebirge than in those from West Eifel, in agreement with the evidence provided by mineral chemistry. An exception is given by CO_2, whose concentration spans over a wide range, especially in olivine-hosted FI (Figg. 7 and S3). In addition, FI in Opx and Cpx from West Eifel xenoliths are richer in volatiles than those from Siebengebirge (only Opx available), further suggesting the superimposition of other processes that reasonably masked the original composition of the residual mantle beneath West Eifel (see Section 6.5) (Figg. 7 and S3). Focusing on $^{4}He/^{40}Ar^*$ of olivine, we highlight that xenoliths from Siebengebirge show $^{4}He/^{40}Ar^*$ in the range 0.50-0.07, that is much lower than in olivine from West Eifel (1.65-0.29) (Fig. 11). This strongly points to a higher degree of melt extraction in the mantle beneath Siebengebirge (up to about 25-30%), while West Eifel shows more fertile (or refertilized) features. This interpretation is further supported by the comparison with $^{4}He/^{40}Ar^*$ measured in olivine from Lower Silesia mantle xenoliths that varied in the range 0.46-0.20 (Fig. 11). Here Matusiak-Małek et al. (2017) and Rizzo et al. (2018), on the basis of mineral chemistry, estimated up to 25-30% of melting from the protolith that left a harzburgitic residuum. This strengthens our interpretation that the mantle beneath Siebengebirge reaches a very refractory compositions, after comparable or even higher extents of melting.

8.3. Metasomatism and refertilization processes

Mineral chemistry data suggest that Opx in some West Eifel and Siebengebirge harzburgites is able to record analogous partial melting degrees (up to 25-30%). On the other hand, the compositional distribution of Cpx and mostly Opx (Figg. 4 and 6) demonstrate that the SCLM portions beneath the two volcanic fields followed different evolutionary paths, likely reflecting a complex history of post-melt extraction enrichment processes. Analogous evidences arise from noble gases systematics in FI, which points out that, after a similar initial depletion, West Eifel mantle was overprinted by complex refertilization/metasomatic events, while

Siebengebirge SCLM was only marginally affected by enrichment processes (Fig. 10). This is also evident from the remarkably higher volatiles (CO_2, N_2*, noble gas) content of FI in pyroxene from West Eifel with respect to those from Siebengebirge (Figg. 7 and S3). The volatiles content in FI suggests that the composition of Cpx and (at least partially) Opx in most of the studied xenoliths from West Eifel is no longer representative of the partial melting history, being modified by the superimposition of metasomatic and/or refertilization processes that caused recrystallization and reasonably entrapment of a newly formed FI population, in most cases CO_2-rich.

If compared to the Mg# of the host minerals, the volatiles content of FI does not follow the typical trend expected for simple partial melting processes (i.e. decreasing at increasing Mg#, Figg. 11 and S3), lying instead on multiple trends with variable ($^{4}He/^{40}Ar$*)/Mg# gradients (Fig. 11a). These behavior, very similar to those identified from the Al_2O_3 and TiO_2 vs. Mg# distribution in Cpx and Opx (Fig. 4), further suggests that one or multiple enrichment events postdated the melt extraction event. Moreover, since the increase of fusible elements and volatiles is recorded only by xenoliths from West Eifel, it is arguable that these metasomatic/refertilization processes were spatially and temporally connected to the Quaternary magmatism of the Eifel area. This is also evident in the $^{3}He/^{4}He$ (Rc/Ra) vs. Mg# diagram (Fig. 11b), where enriched samples lie on a well-defined trend characterized by a progressive decrease of the $^{3}He/^{4}He$ ratio with decreasing Mg#, moving towards the low $^{3}He/^{4}He$ measured in cumulate products (i.e. the olivine-websterite from Gees), as well as in the nowadays gaseous emissions in East Eifel.

A progressive trend from the most depleted Siebengebirge amphibole- and phlogopite-free harzburgites to the enriched West Eifel lithotypes can be also identified by considering the redox and thermal conditions of last equilibrium recorded by the xenoliths. From a theoretical point of view, melt extraction and enrichment processes do not simply correlate with fO_2. Melt extraction is coupled to bulk rock Fe_2O_3 depletion which, in principle, should yield relatively lower $\Delta\log fO_2$ [FMQ] values (e.g., Frost and McCammon, 2008), while enrichments are frequently observed to produce an increase in fO_2 in the SCLM (e.g. Woodland et al., 2006, 1996), although this is not a linear process. In fact, the fO_2 of depleted rocks is easier to raise than that of more fertile rocks, due to the lower amount of spinel (Woodland et al., 2006). More in general, the buffering capacity of depleted peridotites is so low that tiny amounts of metasomatic melts/fluids are sufficient to completely reset the redox state of the system (Stachel and Luth, 2015). In this context, it is arguable that Siebengebirge amphibole- and phlogopite-free harzburgites, which yield the lowest T (880 to 1050°C) conditions, at fO_2 comprised between -0.5 to +1.0 $\Delta\log fO_2$ [FMQ]) (Fig. 6), represent an older portion of the SCLM, predating the onset of metasomatism/refertilization events. Moving towards West Eifel most fertile lithotypes, a gradual increase of T in concomitance with a slight decrease in fO_2 (Fig. 6) highlights that the mantle domains sampled by the Quaternary Eifel volcanism are by far more enriched than those sampled at Siebengebirge between 30 and 6 Ma. In such a framework, West Eifel lherzolites (both anhydrous and amphibole-phlogopite-bearing) do not represent portions of fertile mantle unaffected by melt extraction processes, being rather the refertilization product of refractory, older, "Siebengebirge-like" harzburgites. This is even more evident if the last equilibrium *T* recorded by each sample is compared to the Al_2O_3 (wt%) content of pyroxene or to the $^3He/^4He$ ratio of the FI in the main constituents (olivine and pyroxene) (Fig. 12). Indeed, West Eifel and Siebengebirge harzburgites, i.e. the most refractory samples, are typified by the lowest *T* and Al contents in pyroxene (Fig. 12a), as well as by the highest Rc/Ra ratios in FI (Fig. 12b), being thus interpreted as the coldest and most depleted mantle domains preserving an almost MORB-like signature of $^3He/^4He$. Considering that the $^3He/^4He$ signature of European SCLM is strongly dependent on the extent of crustal recycling, and that the last subduction recorded in the CEVP is Hercynian, we argue that the most refractory domains could represent old portions of lithosphere at an early stage of contamination by subduction-related, U-Th-rich crustal material. It is interesting to notice that similar evidences were observed in the most refractory xenoliths from Lower Silesia (Fig. 10), which is a prolongation of Eger Rift affected by magmatic activity at ~20 Ma, in concomitance with Siebengebirge (Rizzo et al., 2018 and references therein). With increasing fertility of the samples, i.e. moving towards West Eifel lherzolites, the equilibrium *T* and Al content of pyroxene increase and the Rc/Ra ratio decreases (Fig. 12), testifying for the progressive infiltration of hot, Al-rich melts/fluids with $^3He/^4He$ ratio similar to Laacher See gases into the German SCLM. It has however to be noted that a few enriched hydrous phase-bearing samples from Meerfelder Maar also show high Rc/Ra values. This feature could indicate that this portion of SCLM was affected by discontinuous and heterogeneous infiltration of compositionally variable melts with high (asthenosphere-derived?) $^3He/^4He$ signature.

The absence of fertile mantle lithotypes at Siebengebirge enables us to speculate that most of the documented melt/fluid-rock reactions responsible for the modification of the German SCLM took place in a restricted temporal window, being mostly related to the Quaternary magmatic episodes (Lloyd et al., 1991; Witt-Eickschen et al., 1998; Witt and Seck, 1987). Support to this theory is given by the chemical features of mineral phases inside both anhydrous and amphibole-/phlogopite-bearing wehrlites and olivine-clinopyroxenites from West Eifel. As shown in Figure 4, Cpx in these rocks lies along an Al_2O_3 (or TiO_2) vs. Mg# trend that is different from those of lherzolites-harzburgites (higher Al_2O_3/Mg# and TiO_2/Mg# ratios) or olivine-websterites (lower Al_2O_3/Mg# and TiO_2/Mg# ratios). Such a feature, similar to what reported by Coltorti et al. (2020) and Melchiorre et al. (2020) for Antarctica and Patagonia ultramafic xenoliths respectively, testifies for the interaction between depleted mantle and tholeiitic to alkaline melts, i.e. for the occurrence of both metasomatism and refertilization processes within the same SCLM portions. Irrespective of the fact that West Eifel wehrlites could represent cumulates (Witt-Eickschen and Kramm, 1998) or reaction products between depleted dunites, harzburgites or lherzolites and alkaline to carbonated melts (Aulbach et al., 2020; Shaw et al., 2018), the intimate connection between the main metasomatic/refertilization processes and the Quaternary magmatism in the Eifel area is unquestionable. Evidences for the compositional variability of the melts circulating in the German SCLM are also provided by the occurrence of the olivine-websteritic sample at Gees: the compositional peculiarity of pyroxene in this sample (Fig. 4) is counterbalanced by the multiple analogies with most of West Eifel rocks, in terms of both T-fO_2 (Fig. 6) and composition of FI (Figg. 7, 8 and 9). These evidences suggest that minor amounts of SiO_2-saturated to -oversaturated melts were generated in the German SCLM in spatial/temporal association with the main alkaline magmatic phase, confirming what already evidenced by the chemical variability of the outcropping lavas in this area (Wilson and Downes, 1991 and references therein).

8.4. The evolution of the West Eifel and Siebengebirge SCLM

8.4.1. Origin of the noble gas isotopic signature

To constrain the noble gas isotopic signature of the mantle beneath the study area, we put our samples in the context of previous studies on mantle xenoliths from Eifel and from other European areas, in which FI where extracted with the same technique (i.e. in-vacuo crushing). In terms of helium isotopes, we recall that olivine, Opx, and Cpx from West Eifel show $^3He/^4He$ of 5.5-6.7 Ra while those from Siebengebirge show 6.0-6.8 Ra. This range of values is comparable to that found by Gautheron et al. (2005) in olivine from West Eifel (5.5-6.7 Ra) (Fig. 8). More in general, the $^3He/^4He$ signature of the mantle beneath Eifel and Siebengebirge is comparable with that of other European localities (French Massif Central, Kapfenstein, Tallante and Calatrava, Lower Silesia, and Persani Mts.) that varies in the range 5.5-6.9 Ra (Faccini et al., 2020; Gautheron et al., 2005; Martelli et al., 2011; Rizzo et al., 2018). Considering that the magmatism of Siebengebirge is dated at ~30-6 Ma, we argue that the $^3He/^4He$ signature measured in Quaternary Eifel xenoliths can be extended backward in time without any significant variation. As proposed by Gautheron et al. (2005), the European $^3He/^4He$ signature could mostly result from: i) addition into the lithosphere of ^4He-rich fluids/melts derived from U-Th decay of crustal material from dehydration of subducting slabs; ii) mixing between MORB-like astenospheric fluids and more radiogenic fluids circulating in the lithosphere in a steady state condition that could be balanced by either local or global metasomatism. Arguments in support of the second hypothesis relate to a homogeneous $^3He/^4He$ signature found by Gautheron and Moreira (2002) in other worldwide portions of SCLM that include Antarctica. However, more recent studies on mantle xenoliths from other European localities (Faccini et al., 2020; Rizzo et al., 2018) and the West Antarctic Rift System (Correale et al., 2019 and references therein) that integrate the study of noble gas in FI with the petrography and mineral chemistry of the rocks highlight that the $^3He/^4He$ range of SCLM of non-cratonic areas is wider than previously thought and local heterogeneities must be considered in response to the geodynamics. We think it is more reasonable to hypothesize that the steady state model proposed by Gautheron et al. (2005) involves the circulation of ^4He-rich fluids/melts derived from U-Th decay of crustal material from dehydration of subducting slabs rather than a simple U-Th radioactivity in the lithosphere. This is also supported by the lowest $^{3}He/^{4}He$ values in Europe, that are found in Persani Mts. (Transylvania; 5.8±0.2 Ra) and Tallante (Spain; 5.6±0.1 Ra) where recent subduction has occurred (Faccini et al., 2020; Martelli et al., 2011) (Fig. 8). On the other hand, the highest $^{3}He/^{4}He$ values are generally found in metasomatized/refertilized Cpx and Opx, suggesting that MORB-like astenospheric fluids mixed with those more contaminated residing in the SCLM (Faccini et al., 2020; Rizzo et al., 2018) and that the most refractory samples from Siebengebirge and West Eifel could represent early stages of mantle contamination by crustal fluids derived from Hercynian subduction (Fig. 11).

Regarding the origin of neon and argon, as discussed in Section 6.3.1 $^{20}Ne/^{22}Ne$ and $^{21}Ne/^{22}Ne$ as well as $^{40}Ar/^{36}Ar$ and $^{3}He/^{36}Ar$ reflect a contamination by atmosphere-derived fluids (Fig. 9). In fact, data from West Eifel and Siebengebirge fall along the theoretical air-MORB mixing line defined for neon by Sarda et al. (1988) and Moreira et al. (1998) ($^{21}Ne/^{22}Ne$ = 0.06 and $^{20}Ne/^{22}Ne$ = 12.5) and for argon by Moreira et al. (1998) and Ballentine et al. (2005) ($^{40}Ar/^{36}Ar$ up to 44,000 and $^{3}He/^{36}Ar$~0.45) (Fig. 9). Similar indications were found by Gautheron et al. (2005) in other mantle xenoliths from Eifel and other European localities, although these authors inferred that the $^{3}He/^{36}Ar$ variability they found in olivine could be due to preferential loss of helium from the FI into the matrix of the mineral grains. We disagree with this interpretation, arguing that the $^{3}He/^{36}Ar$ variability observed at constant $^{40}Ar/^{36}Ar$ depends on the distinct $^{4}He/^{40}Ar^{*}$ and $^{3}He/^{4}He$ that characterized each xenolith and mineral phase. We base our considerations on the integration of mineral chemistry with FI composition of noble gases in the same xenoliths. Similar observations were made in other recent studies in European localities (Faccini et al., 2020; Rizzo et al., 2018). Moreover, a preferential loss of helium should induce an isotopic fractionation, with a decrease of $^{3}He/^{4}He$ that is not observed (see also Faccini et al., 2020). This implies that the original Ne and Ar isotopic signature of the mantle beneath Eifel and Siebengebirge can be considered as MORB-like.

8.4.2. The evolution of the CEVP lithosphere and the source of the magmatism

The nature and evolution of the SCLM beneath Eifel, Siebengebirge and the whole CEVP is a hotly debated topic, intimately related to the ongoing discussion about the presence of one or multiple mantle plumes beneath central Europe. In terms of noble gases systematics, a plume-related signature is expressed by $^{3}He/^{4}He$ values above the MORB range (>9 Ra), a lower $^{21}Ne/^{22}Ne$ ratio for a given $^{20}Ne/^{22}Ne$ than MORB melts, and $^{40}Ar/^{36}Ar$ in the range of 5,000-10,000 (Allègre et al., 1987; Colin et al., 2015; Kurz et al., 2009; Moreira, 2013; Mukhopadhyay, 2012). Our study shows that He, Ne, and Ar isotopic ratios measured in ultramafic xenoliths from West Eifel and Siebengebirge (Figg. 8 and 9) are compatible with a mixing between crustal- (for He isotopes) and/or atmosphere-derived (for Ne and Ar isotopes) and MORB-like fluids (Bekaert et al., 2019; Bräuer et al., 2013; Faccini et al., 2020; Gautheron et al., 2005; Moreira et al., 2018;

Rizzo et al., 2018), thus precluding the presence of a plume below the area. Our results are in contrast with the few geochemical studies of noble gases in mantle xenoliths or in surface gases from Eifel that support the hypothesis of a plume beneath this area (Buikin et al., 2005; Caracausi et al., 2016; Trieloff and Altherr, 2007). Instead, our data are more consistent with the model proposed by Lustrino and Carminati (2007), according to whom the origin of European Cenozoic volcanism should be ascribed to crustal extension and melting of the lithospheric mantle and/or passive asthenosphere upwelling driven by decompression. According to our findings, the SCLM portion sampled by Siebengebirge magmas was strongly depleted in terms of both major elements and volatiles content, being a candidate to represent the German lithosphere prior to the massive infiltration of melts/fluids belonging to the Quaternary Eifel volcanism. On the other hand, ultramafic xenoliths from West Eifel record a complex history of melt/fluid-rock reactions (see also Aulbach et al., 2020; Shaw et al., 2018). The large compositional variability of this latter xenoliths suite is ascribable to the infiltration of multiple metasomatising/refertilizing agents, and suggests that both tholeiitic and alkaline melts could have been circulating in the SCLM. Although our model cannot be constrained in terms of absolute ages, we are prone to believe that the modal and compositional enrichment of West Eifel xenoliths have to be ascribed to relatively young metasomatism/refertilization processes, taking place between the end of the Siebengebirge volcanism and the Quaternary Eifel magmatism itself, i.e. at least between ~6 and ~0.5 Ma. Such a model would be capable of explaining why the mantle beneath Siebengebirge, unaffected by Quaternary metasomatism/refertilization processes, is mainly composed of amphibole- and phlogopite-free domains with refractory composition, recording relatively low T and fO_2 conditions. In this view, multiple generations of amphibole in West Eifel xenoliths, ascribed by some authors to metasomatic episodes with Carboniferous to Quaternary ages (Shaw et al., 2005; Witt-Eickschen et al., 2003), would be confined to recent heterogeneous metasomatism/refertilization processes affecting the German SCLM in a restricted time interval, fitting the alternative hypothesis proposed by the same authors (Witt-Eickschen et al., 2003).

8.5. Comparison with gases emitted in the Eifel volcanic field

The Eifel volcanic area is nowadays characterized by the occurrence of many CO_2-rich mineral springs and mofettes, from which the emission of helium with mantle-derived fingerprint pointed to the existence of still active magmatic reservoir beneath the region (e.g., Aeschbach-Hertig et al., 1996; Bekaert et al., 2019; Bräuer et al., 2011, 2005; Giggenbach et al., 1991; Griesshaber et al., 1992). Most of these gas emissions and especially those showing the highest $^3He/^4He$ signature are nearly pure CO_2 and occur in the East Eifel, in an area of ~10 km^2 that is bordered by the Rieden, Wehr and Laacher See calderas (Aeschbach-Hertig et al., 1996; Bräuer et al., 2013, 2005; Giggenbach et al., 1991; Griesshaber et al., 1992). Wehr gases are typified by the highest $^3He/^4He$ (up to 5.7 Ra; Bräuer et al., 2013; Griesshaber et al., 1992), Ne-Ar isotopic ratios close to atmospheric values (i.e., $^{20}Ne/^{22}Ne$=9.7-10.1, $^{21}Ne/^{22}Ne$=0.027-0.030, and $^{40}Ar/^{36}Ar$=307-565), and $^{4}He/^{40}Ar^{*}$ of 0.4-1.5 (Bräuer et al., 2013). However, the most famous and studied gas emissions are those from Laacher See, which is the result of the most recent volcanic eruption, occurred in the East Eifel about 11 ka ago (Zolitschka et al., 1995). These gases are discharged along the eastern shore and from the bottom of the maar lake (Aeschbach-Hertig et al., 1996; Giggenbach et al., 1991). The chemistry of these emissions is made of nearly pure CO_2, as in Wehr gases, with Ne-Ar isotopic ratios close to atmospheric values (i.e., $^{20}Ne/^{22}Ne$=9.7-10.0, $^{21}Ne/^{22}Ne$=0.027-0.030, and $^{40}Ar/^{36}Ar$=314-391), $^{4}He/^{40}Ar^{*}$ of 1.1-3.0 and $^{3}He/^{4}He$ in the narrow range of 5.1-5.6 Ra that is almost constant since 1988, indicating a reduced magmatic activity (Aeschbach-Hertig et al., 1996; Bräuer et al., 2013, 2005; Giggenbach et al., 1991; Griesshaber et al., 1992). Bräuer et al. (2013, 2011) argued that this behaviour contrasts with that of gases emitted from Bublák mofette (Cheb Basin) in the NW Bohemian Rift, where $^{3}He/^{4}He$ values are higher than in Eifel (up to 6.3 Ra) and varied significantly in the last decades in response to an inferred magmatic activity and an observed intra-crustal seismicity. Gas emissions from West Eifel are scarcer than in East Eifel and, although are equally made of nearly pure CO_2, are characterized by low $^{3}He/^{4}He$ (2.6 Ra at well Wallenborn) as well as a low air contamination (i.e., $^{20}Ne/^{22}Ne$ up to 11.2 and $^{40}Ar/^{36}Ar$=1,060) indicating that magmatic gases are contaminated by crustal fluids (Griesshaber et al., 1992). In the southern part of West Eifel, but outside the main volcanic area, gases made of almost pure CO_2 are emitted from two wells (Victoriaquelle and Schwefelquelle) that show $^{3}He/^{4}He$ of 4.2-4.5 Ra, $^{20}Ne/^{22}Ne$ up to 11.2, $^{21}Ne/^{22}Ne$ up to 0.046, $^{40}Ar/^{36}Ar$ up to 8,287, and $^{4}He/^{40}Ar^{*}$ of 0.6-1.3 (Bekaert et al., 2019; Bräuer et al., 2013; Caracausi et al., 2016). Bräuer et al. (2013) argued that the differences in the $^{3}He/^{4}He$ values between East and West Eifel areas can be explained with the existence of at least two distinct magmatic systems with different melt composition, different gas/melt fractions and/or different age.

The new $^{3}He/^{4}He$ and $^{4}He/^{40}Ar^{*}$ data in FI from ultramafic xenoliths from West Eifel and Siebengebirge presented in our study enable to discriminate between melt extraction and enrichment processes in the SCLM and to distinguish between mantle- and magmatic-derived (cumulate) xenoliths, but also offer the opportunity to put forwards a comparison with the isotopic signature measured in surface gases. Olivine, Opx, and Cpx from West Eifel show $^{3}He/^{4}He$ of 5.5-6.7 Ra, 5.5-6.5 Ra, and 5.6-6.7 Ra, respectively, while those from Siebengebirge show 6.02-6.80 in olivine and 6.03-6.80 in Opx (it was not possible to make measurements on Cpx). Xenoliths of cumulate origin (MM1, GE1, and DBR2) were only found in West Eifel and show $^{3}He/^{4}He$ of 5.5-6.3 Ra and $^{4}He/^{40}Ar^{*}$ of 0.5-4.0 (Table S5), decreasing with decreasing Mg# (Fig. 11). These evidences suggest that gases emitted from East Eifel are not perfectly representative of the $^{3}He/^{4}He$ signature of the SCLM beneath this area, which has a higher isotopic signature and is comparable to that of Eger Rift (Bräuer et al., 2011; Rizzo et al., 2018). In this view, the surface gases probably suffer a slight contamination by crustal fluids or reflect magma ageing in the reservoir from which they are degassed.

Instead, the range of $^4He/^{40}Ar^*$ measured in cumulate xenoliths (0.5-4.0), which should be indicative of the degassing pressure and extent (e.g., Boudoire et al., 2018), perfectly matches that of surface gases (0.4-3.0) supporting the idea that the latter are degassed from a magma residing at the Moho depth (Bräuer et al., 2013).

9. Summary and conclusions

A coupled study of petrographic features, mineral chemistry and noble gases plus CO_2 in FI from ultramafic xenoliths hosted in West Eifel and Siebengebirge volcanic fields (Germany) allowed to define the main features of this portion of the European SCLM and to reconstruct its temporal evolution. The main results can be summarized as follows:

- The xenoliths from West Eifel (Meerfelder Maar, Dreiser Weiher, Gees) are generally lherzolites, harzburgites and wehrlites, often amphibole- and phlogopite-bearing. Few olivine-clinopyroxenites and one olivine-websterite are also present. Olivine has a large compositional variation (83.4-91.6 Fo; 0.16-0.42 wt% NiO), especially between the typical mantle lithologies (harzburgites and lherzolites) and those of different origin (reaction products and/or cumulates). Siebengebirge (Willmeroth and Eulenberg) rocks are mostly amphibole- and phlogopite-free harzburgites with very restitic compositions (olivine Fo = 90.5-91.8; NiO = 0.31-0.43 wt%), typical of depleted lithologies.
- Major element distribution in Opx suggest that xenoliths from West Eifel record limited melt extraction (except harzburgites from Gees, which record up to 25-30% partial melting), followed by predominant enrichment processes. On the other hand, Siebengebirge xenoliths represent mantle residua after significant melt extraction (>20% partial melting).
- The variable Al-Ti-enrichment of pyroxene and high *T* of last equilibration recorded by West Eifel xenoliths are consistent with the occurrence of one or multiple metasomatism/refertilization processes. The absence of modal enrichment in Siebengebirge rocks led us to hypothesize that metasomatism and/or refertilization took place in a time span comprised between 6 Ma (end of Siebengebirge magmatic cycle) and ~0.5-0.01 Ma (age of West Eifel magmatism), being thus related to the ultimate mobilization of melt/fluids in the German SCLM.
- Two main FI genetic types (primary vs. secondary) are present in West Eifel and Siebengebirge xenoliths and occur in all the studied phases, especially in association with intergranular reaction zones. The chemistry of FI is dominated by CO_2, with N_2 being the second-most-abundant species. Most of FI in olivine belong to a residual mantle depleted after various episodes of melt extractions, while FI in Opx and Cpx record overprinting by at least one metasomatic/refertilization event postdating the partial melting.

- The $^3He/^4He$ ratios in mineral phases from West Eifel are between 5.5 and 6.7 Ra, while those from Siebengebirge are 6.0-6.8 Ra. These values are comparable to those found by Gautheron et al. (2005) in olivine only from Quaternary West Eifel (5.5-6.7 Ra) and that of other European localities (5.5-6.9 Ra; Faccini et al., 2020; Gautheron et al., 2005; Martelli et al., 2011; Rizzo et al., 2018).
- The systematics of Ne and Ar isotopes indicate that most of the data are consistent with mixing between a recycled air component and a MORB-like mantle. This evidence, together with that from the measured $^3He/^4He$ ratios, excludes the presence of a classical plume of the lower mantle beneath the study area and the other localities belonging to CEVP. The geochemistry of FI results from a mixing of two endmembers: (1) the residual mantle, resulting from partial melting of European SCLM characterized by the recycling of crustal- and atmosphere-derived material from dehydration of fossil or recent slabs, and (2) an asthenosphere-derived refertilizing/metasomatising agent, variably enriched in CO_2 and originally characterized by MORB-like $^3He/^4He$ ratios.
- Some xenoliths from West Eifel show cumulate features as indicated by mineral chemistry as well as by $^3He/^4He$ and $^4He/^{40}Ar^*$ values that tend toward the range of values measured in magmatic gases emitted at the surface.
- The negative correlation between Rc/Ra values and both equilibration *T* and increasing Al content of pyroxene (Fig. 12) suggests that the most refractory and ancient domains of the German mantle could have a MORB-like $^3He/^4He$ signature that have been contaminated by subduction-related, U-Th-rich crustal material. According to our findings, melts/fluids-related metasomatism and/or refertilization events affected the German SCLM in concomitance with the development of Quaternary magmatism in the Eifel area. The compositional heterogeneities of ultramafic xenoliths in West Eifel and Siebengebirge is thus the result of heterogeneous enrichment processes, likely associated to the circulation of both tholeiitic and alkaline melts in the SCLM in a restricted time interval.

Author Contributions Statement

A.L.R. and M.C. collected samples; T.N., B.F. and F.C. prepared thin sections. A.L.R. and B.F. handpicked minerals from mantle xenoliths; A.L.R. performed analyses of fluid inclusions, participated in mineral chemistry analyses, elaborated and interpreted data, conceptualized models, and drafted the manuscript and edited the final version; B.F., M.C., F.C., and L.F. elaborated and interpreted petrography and mineral chemistry data, as well as assisted in writing the manuscript; T.N. performed mineral chemistry analyses, and helped in petrography and mineral chemistry data interpretation; M.C., B.F., F.C., L.F., T.N., and F.I. provided constructive comments on and edited the final version of the manuscript.

Funding

A.L.R. acknowledges financial support from Università degli Studi di Ferrara for the 2017, 2018, and 2019 IUSS international mobility program during his PhD, as well as INGV-Palermo and the University of Vienna for providing analytical facilities, and Italian Ministero Istruzione Università e Ricerca (PRIN Grants 2017LMNLAW to [A.L.R.] and 20178LPCPW to [M.C.]).

Conflict of Interest Statement

The authors declare that the research was conducted in the absence of any commercial or financial relationships that could be construed as potential conflicts of interest.

Acknowledgments

This work is part of the PhD (XXXII cycle) of Andrea Luca Rizzo at the University of Ferrara. We thank Mariagrazia Misseri and Mariano Tantillo for helping in sample preparation, in INGV-Palermo laboratory activities, and in the isotope analysis of noble gases. We are also grateful to Matthias Ghiotto and Andrea Buian for helping in minerals hand-picking, as well as Andres Libardo Sandoval Velasquez for sample preparation finalized to the extraction of CO_2 from fluid inclusions.

References

Aeschbach-Hertig, W., Kipfer, R., Hofer, M., Imboden, D.M., Wieler, R., Signer, P., 1996. Quantification of gas fluxes from the subcontinental mantle: The example of Laacher See, a maar lake in Germany. Geochim. Cosmochim. Acta 60, 31–41. https://doi.org/10.1016/0016-7037(95)00370-3

Allègre, C.J., Staudacher, T., Sarda, P., 1987. Rare gas systematics: formation of the atmosphere, evolution and structure of the Earth's mantle. Earth Planet. Sci. Lett. 81, 127–150. https://doi.org/10.1016/0012-821X(87)90151-8

Arai, S., 1994. Characterization of spinel peridotites by olivine-spinel compositional relationships: Review and interpretation. Chem. Geol. 113, 191–204. https://doi.org/10.1016/0009-2541(94)90066-3

Aulbach, S., Lin, A.-B., Weiss, Y., Yaxley, G.M., 2020. Wehrlites from continental mantle monitor the passage and degassing of carbonated melts. Geochemical Perspect. Lett. 15, 30–34. https://doi.org/10.7185/geochemlet.2031

Bailey, D.K., 1978. Continental Rifting and Mantle Degassing, in: Neumann, E.-R., Ramberg, I.B. (Eds.), Petrology and Geochemistry of Continental Rifts. Springer Netherlands, Dordrecht, pp. 1–13. https://doi.org/10.1007/978-94-009-9803-2_1

Ballentine, C.J., 1997. Resolving the mantle He/Ne and crustal $^{21}Ne/^{22}Ne$ in well gases. Earth Planet. Sci. Lett. 152, 233–249. https://doi.org/10.1016/s0012-821x(97)00142-8

Ballentine, C.J., Marty, B., Lollar, B.S., Cassidy, M., 2005. Neon isotopes constrain convection and volatile origin in the Earth's mantle. Nature 433, 33–38. https://doi.org/10.1038/nature03182

Ballhaus, C., Berry, R.F., Green, D.H., 1991. High pressure experimental calibration of the olivine-orthopyroxene-spinel oxygen geobarometer: implications for the oxidation state of the upper mantle. Contrib. to Mineral. Petrol. 107, 27–40. https://doi.org/10.1007/BF00311183

Ban, M., Witt-Eickschen, G., Klein, M., Seck, H.A., 2005. The origin of glasses in hydrous mantle xenoliths from the West Eifel, Germany: incongruent break down of amphibole. Contrib. to Mineral. Petrol. 148, 511–523. https://doi.org/10.1007/s00410-004-0623-x

Bekaert, D. V, Broadley, M.W., Caracausi, A., Marty, B., 2019. Novel insights into the degassing history of Earth's mantle from high precision noble gas analysis of magmatic gas. Earth Planet. Sci. Lett. 525, 115766. https://doi.org/10.1016/j.epsl.2019.115766

Bénard, A., Woodland, A.B., Arculus, R.J., Nebel, O., McAlpine, S.R.B., 2018. Variation in sub-arc mantle oxygen fugacity during partial melting recorded in refractory peridotite xenoliths from the West Bismarck Arc. Chem. Geol. 486, 16–30. https://doi.org/10.1016/j.chemgeo.2018.03.004

Bonadiman, C., Coltorti, M., 2011. Numerical modelling for peridotite phase melting trends in the SiO_2-Al_2O_3-FeO-MgO-CaO system at 2 GPa. Mineral. Mag. 75, 548.

Boudoire, G., Rizzo, A.L., Di Muro, A., Grassa, F., Liuzzo, M., 2018. Extensive CO_2 degassing in the upper mantle beneath oceanic basaltic volcanoes: First insights from Piton de la Fournaise volcano (La Réunion Island). Geochim. Cosmochim. Acta 235, 376–401. https://doi.org/10.1016/j.gca.2018.06.004

Bräuer, K., Kämpf, H., Koch, U., Strauch, G., 2011. Monthly monitoring of gas and isotope compositions in the free gas phase at degassing locations close to the Nový Kostel focal zone in the western Eger Rift, Czech Republic. Chem. Geol. 290, 163–176. https://doi.org/10.1016/j.chemgeo.2011.09.012

Bräuer, K., Kämpf, H., Niedermann, S., Strauch, G., 2013. Indications for the existence of different magmatic reservoirs beneath the Eifel area (Germany): A multi-isotope (C, N, He, Ne, Ar) approach. Chem. Geol. 356, 193–208. https://doi.org/10.1016/j.chemgeo.2013.08.013

Bräuer, K., Kämpf, H., Niedermann, S., Strauch, G., 2005. Evidence for ascending upper mantle-derived melt beneath the Cheb basin, central Europe. Geophys. Res. Lett. 32, 1–4. https://doi.org/10.1029/2004GL022205

Bryndzia, L.T., Wood, B.J., 1990. Oxygen thermobarometry of abyssal spinel peridotites: the redox state and C-O-H volatile composition of the Earth's sub-oceanic upper mantle. Am. J. Sci. 290, 1093–1116. https://doi.org/10.2475/ajs.290.10.1093

Buikin, A., Trieloff, M., Hopp, J., Althaus, T., Korochantseva, E., Schwarz, W.H., Altherr, R., 2005. Noble gas isotopes suggest deep mantle plume source of late Cenozoic mafic alkaline volcanism in Europe. Earth Planet. Sci. Lett. 230, 143–162. https://doi.org/10.1016/j.epsl.2004.11.001

Burnard, P., 2004. Diffusive fractionation of noble gases and helium isotopes during mantle melting. Earth Planet. Sci. Lett. 220, 287–295. https://doi.org/10.1016/S0012-821X(04)00060-3

Burnard, P.G., Farley, K.A., Turner, G., 1998. Multiple fluid pulses in a Samoan harzburgite. Chem. Geol. 147, 99–114. https://doi.org/10.1016/S0009-2541(97)00175-7

Canil, D., O'Neill, H.S.C., 1996. Distribution of ferric iron in some upper-mantle assemblages. J. Petrol. 37, 609–635. https://doi.org/10.1093/petrology/37.3.609

Caracausi, A., Avice, G., Burnard, P.G., Füri, E., Marty, B., 2016. Chondritic xenon in the Earth's mantle. Nature 533, 82–85. https://doi.org/10.1038/nature17434

Casetta, F., Ickert, R.B., Mark, D.F., Bonadiman, C., Giacomoni, P.P., Ntaflos, T., Coltorti, M., 2019. The alkaline lamprophyres of the dolomitic area (Southern Alps, Italy): Markers of the Late Triassic change from orogenic-like to anorogenic magmatism. J. Petrol. 60, 1263–1298. https://doi.org/10.1093/petrology/egz031

Casetta, F., Ickert, R.B., Mark, D.F., Giacomoni, P.P., Bonadiman, C., Ntaflos, T., Zanetti, A., Coltorti, M., 2020. The Variscan subduction inheritance in the Southern Alps Sub-Continental Lithospheric Mantle: Clues from the Middle Triassic shoshonitic magmatism of the Dolomites (NE Italy). Lithos 105856. https://doi.org/10.1016/j.lithos.2020.105856

Colin, A., Moreira, M., Gautheron, C., Burnard, P., 2015. Constraints on the noble gas composition of the deep mantle by bubble-by-bubble analysis of a volcanic glass sample from Iceland. Chem. Geol. 417, 173–183. https://doi.org/10.1016/j.chemgeo.2015.09.020

Coltorti, M., Bonadiman, C., Casetta, F., Faccini, B., Giacomoni, P.P., Pelorosso, B., Perinelli, C., 2020. Nature and evolution of the Northern Victoria Land Lithospheric Mantle (Antarctica). Geol. Soc. London Memoirs: the Antarctic mantle. In press.

Correale, A., Martelli, M., Paonita, A., Rizzo, A., Brusca, L., Scribano, V., 2012. New evidence of mantle heterogeneity beneath the Hyblean Plateau (southeast Sicily, Italy) as inferred from noble gases and geochemistry of ultramafic xenoliths. Lithos 132–133, 70–81. https://doi.org/10.1016/j.lithos.2011.11.007

Correale, A., Pelorosso, B., Rizzo, A.L., Coltorti, M., Italiano, F., Bonadiman, C., Giacomoni, P.P., 2019. The nature of the West Antarctic Rift System as revealed by noble gases in mantle minerals. Chem. Geol. 524, 104–118. https://doi.org/10.1016/j.chemgeo.2019.06.020

Correale, A., Rizzo, A.L., Barry, P.H., Lu, J., Zheng, J., 2016. Refertilization of lithospheric mantle beneath the Yangtze craton in south-east China: Evidence from noble gases geochemistry. Gondwana Res. 38, 289–303. https://doi.org/10.1016/j.gr.2016.01.003

Dèzes, P., Schmid, S.M., Ziegler, P.A., 2004. Evolution of the European Cenozoic Rift System: Interaction of the Alpine and Pyrenean orogens with their foreland lithosphere. Tectonophysics 389, 1–33.

https://doi.org/10.1016/j.tecto.2004.06.011
Dick, H.J.B., Bullen, T., 1984. Chromian spinel as a petrogenetic indicator in abyssal and alpine-type peridotites and spatially associated lavas. Contrib. to Mineral. Petrol. 86, 54–76. https://doi.org/10.1007/BF00373711
Ernst, A., Bohatý, J., 2009. Schischcatella (Fenestrata, Bryozoa) from the devonian of the Rhenish Massif, Germany. Palaeontology 52, 1291–1310. https://doi.org/10.1111/j.1475-4983.2009.00899.x
Faccini, B., Rizzo, A.L., Bonadiman, C., Ntaflos, T., Seghedi, I., Grégoire, M., Ferretti, G., Coltorti, M., 2020. Subduction-related melt refertilisation and alkaline metasomatism in the Eastern Transylvanian Basin lithospheric mantle: Evidence from mineral chemistry and noble gases in fluid inclusions. Lithos 364–365, 105516. https://doi.org/10.1016/j.lithos.2020.105516
Foley, S.F., Fischer, T.P., 2017. An essential role for continental rifts and lithosphere in the deep carbon cycle. Nat. Geosci. 10, 897–902. https://doi.org/10.1038/s41561-017-0002-7
Frechen, J., Vieten, K., 1970a. Petrographie der Vulkanite des Siebengebirges. Die peralkalische Gesteinsreihe Alkalitrachyt-Sanidinbasanit. Decheniana 122, 357–377.
Frechen, J., Vieten, K., 1970b. Petrographie der Vulkanite des Siebengebirges. Die subalkalische Gesteinsreihe Quarztrachyt-Latitbasalt. Decheniana 122, 337–356.
Frost, D.J., McCammon, C.A., 2008. The Redox State of earth's mantle. Annu. Rev. Earth Planet. Sci. 36, 389–420. https://doi.org/10.1146/annurev.earth.36.031207.124322
Gautheron, C., Moreira, M., 2002. Helium signature of the subcontinental lithospheric mantle. Earth Planet. Sci. Lett. 199, 39–47. https://doi.org/10.1016/S0012-821X(02)00563-0
Gautheron, C., Moreira, M., Allègre, C., 2005. He, Ne and Ar composition of the European lithospheric mantle. Chem. Geol. 217, 97–112. https://doi.org/10.1016/j.chemgeo.2004.12.009
Gennaro, M.E., Grassa, F., Martelli, M., Renzulli, A., Rizzo, A.L., 2017. Carbon isotope composition of CO_2-rich inclusions in cumulate-forming mantle minerals from Stromboli volcano (Italy). J. Volcanol. Geotherm. Res. 346, 95–103. https://doi.org/10.1016/j.jvolgeores.2017.04.001
Giacomoni, P.P., Bonadiman, C., Casetta, F., Faccini, B., Ferlito, C., Ottolini, L., Zanetti, A., Coltorti, M., 2020. Long-term storage of subduction-related volatiles in Northern Victoria Land lithospheric mantle: Insight from olivine-hosted melt inclusions from McMurdo basic lavas (Antarctica). Lithos 378–379, 105826. https://doi.org/10.1016/j.lithos.2020.105826
Giggenbach, W.F., Sano, Y., Schmincke, H.U., 1991. CO_2-rich gases from Lakes Nyos and Monoun, Cameroon; Laacher See, Germany; Dieng, Indonesia, and Mt. Gambier, Australia-variations on a common theme. J. Volcanol. Geotherm. Res. 45, 311–323. https://doi.org/10.1016/0377-0273(91)90065-8
Graham, D.W., 2002. Noble Gas Isotope Geochemistry of Mid-Ocean Ridge and Ocean Island Basalts:

Characterization of Mantle Source Reservoirs. Rev. Mineral. Geochemistry 47, 247–317. https://doi.org/10.2138/rmg.2002.47.8

Griesshaber, E., O'Nions, R.K., Oxburgh, E.R., 1992. Helium and carbon isotope systematics in crustal fluids from the Eifel, the Rhine Graben and Black Forest, F.R.G. Chem. Geol. 99, 213–235. https://doi.org/10.1016/0009-2541(92)90178-8

Gurenko, A.A., Hoernle, K.A., Hauff, F., Schmincke, H.U., Han, D., Miura, Y.N., Kaneoka, I., 2006. Major, trace element and Nd-Sr-Pb-O-He-Ar isotope signatures of shield stage lavas from the central and western Canary Islands: Insights into mantle and crustal processes. Chem. Geol. 233, 75–112. https://doi.org/10.1016/j.chemgeo.2006.02.016

Harrison, D., Barry, T., Turner, G., 2004. Possible diffusive fractionation of helium isotopes in olivine and clinopyroxene phenocrysts. Eur. J. Mineral. 16, 213–220. https://doi.org/10.1127/0935-1221/2004/0016-0213

Heber, V.S., Brooker, R.A., Kelley, S.P., Wood, B.J., 2007. Crystal-melt partitioning of noble gases (helium, neon, argon, krypton, and xenon) for olivine and clinopyroxene. Geochim. Cosmochim. Acta 71, 1041–1061. https://doi.org/10.1016/j.gca.2006.11.010

Heber, V.S., Wieler, R., Baur, H., Olinger, C., Friedmann, T.A., Burnett, D.S., 2009. Noble gas composition of the solar wind as collected by the Genesis mission. Geochim. Cosmochim. Acta 73, 7414–7432. https://doi.org/10.1016/j.gca.2009.09.013

Herzberg, C., Vidito, C., Starkey, N.A., 2016. Nickel-cobalt contents of olivine record origins of mantle peridotite and related rocks. Am. Mineral. 101, 1952–1966. https://doi.org/10.2138/am-2016-5538

Hilton, D.R., Fischer, T.P., Marty, B., 2002. Noble Gases and Volatile Recycling at Subduction Zones. Rev. Mineral. Geochemistry 47, 319–370. https://doi.org/10.2138/rmg.2002.47.9

Hilton, D.R., Gronvold, K., Sveinbjornsdottir, A.E., Hammerschmidt, K., 1998. Helium isotope evidence for off-axis degassing of the Icelandic hotspot. Chem. Geol. 149, 173–187. https://doi.org/10.1016/S0009-2541(98)00044-8

Hilton, D.R., Hammerschmidt, K., Teufel, S., Friedrichsen, H., 1993. Helium isotope characteristics of Andean geothermal fluids and lavas. Earth Planet. Sci. Lett. 120, 265–282. https://doi.org/10.1016/0012-821X(93)90244-4

Johnson, K.T.M., Dick, H.J.B., Shimizu, N., 1990. Melting in the oceanic upper mantle: an ion microprobe study of diopsides in abyssal peridotites. J. Geophys. Res. 95, 2661–2678. https://doi.org/10.1029/JB095iB03p02661

Kempton, P.D., Harmon, R.S., Stosch, H.G., Hoefs, J., Hawkesworth, C.J., 1988. Open-system O-isotope behaviour and trace element enrichment in the sub-Eifel mantle. Earth Planet. Sci. Lett. 89, 273–287. https://doi.org/10.1016/0012-821X(88)90116-1

Keyser, M., Ritter, J.R.R., Jordan, M., 2002. 3D shear-wave velocity structure of the Eifel plume, Germany. Earth Planet. Sci. Lett. 203, 59–82. https://doi.org/10.1016/S0012-821X(02)00861-0

Kolb, M., Paulick, H., Kirchenbaur, M., Münker, C., 2012. Petrogenesis of mafic to felsic lavas from the oligocene siebengebirge volcanic field (Germany): Implications for the origin of intracontinental volcanism in central Europe. J. Petrol. 53, 2349–2379. https://doi.org/10.1093/petrology/egs053

Kurz, M.D., 1986. Cosmogenic helium in a terrestrial igneous rock. Nature 320, 435–439. https://doi.org/10.1038/320435a0

Kurz, M.D., Curtice, J., Fornari, D., Geist, D., Moreira, M., 2009. Primitive neon from the center of the Galápagos hotspot. Earth Planet. Sci. Lett. 286, 23–34. https://doi.org/10.1016/j.epsl.2009.06.008

Lippolt, H.J., 1983. Distribution of Volcanic Activity in Space and Time, in: Fuchs, K., von Gehlen, K., Mälzer, H., Murawski, H., Semmel, A. (Eds.), Plateau Uplift. Springer Berlin Heidelberg, Berlin, Heidelberg, pp. 112–120. https://doi.org/10.1007/978-3-642-69219-2_15

Lloyd, F.E., Edgar, A.D., Forsyth, D.M., Barnett, R.L., 1991. The paragenesis of upper-mantle xenoliths from the Quaternary volcanics south-east of Gees, West Eifel, Germany. Mineral. Mag. 55, 95–112. https://doi.org/10.1180/minmag.1991.055.378.08

Lustrino, M., Carminati, E., 2007. Phantom plumes in Europe and the circum-Mediterranean region, in: Special Paper of the Geological Society of America. Geological Society of America, pp. 723–745. https://doi.org/10.1130/2007.2430(33)

Lustrino, M., Wilson, M., 2007. The circum-Mediterranean anorogenic Cenozoic igneous province. Earth-Science Rev. 81, 1–65. https://doi.org/10.1016/j.earscirev.2006.09.002

Martelli, M., Bianchini, G., Beccaluva, L., Rizzo, A., 2011. Helium and argon isotopic compositions of mantle xenoliths from Tallante and Calatrava, Spain. J. Volcanol. Geotherm. Res. 200, 18–26. https://doi.org/10.1016/j.jvolgeores.2010.11.015

Martelli, M., Rizzo, A.L., Renzulli, A., Ridolfi, F., Arienzo, I., Rosciglione, A., 2014. Noble-gas signature of magmas from a heterogeneous mantle wedge: The case of Stromboli volcano (Aeolian Islands, Italy). Chem. Geol. 368, 39–53. https://doi.org/10.1016/j.chemgeo.2014.01.003

Marty, B., 2012. The origins and concentrations of water, carbon, nitrogen and noble gases on Earth. Earth Planet. Sci. Lett. 313–314, 56–66. https://doi.org/10.1016/j.epsl.2011.10.040

Matsumoto, T., Chen, Y., Matsuda, J.I., 2001. Concomitant occurence of primordial and recycled noble gasesin the Earth's mantle. Earth Planet. Sci. Lett. 185, 35–47. https://doi.org/10.1016/S0012-821X(00)00375-7

Matsumoto, T., Honda, M., McDougall, I., O'Reilly, S.Y., 1998. Noble gases in anhydrous lherzolites from the Newer Volcanics, southeastern Australia: A MORB-like reservoir in the subcontinental mantle. Geochim. Cosmochim. Acta 62, 2521–2533. https://doi.org/10.1016/S0016-7037(98)00173-2

Matsumoto, T., Honda, M., McDougall, I., O'Reilly, S.Y., Norman, M., Yaxley, G., 2000. Noble gases in pyroxenites and metasomatised peridotites from the Newer Volcanics, southeastern Australia: Implications for mantle metasomatism. Chem. Geol. 168, 49–73. https://doi.org/10.1016/S0009-2541(00)00181-9

Matsumoto, T., Pinti, D.L., Matsuda, J.I., Umino, S., 2002. Recycled noble gas and nitrogen in the subcontinental lithospheric mantle: Implications from N-He-Ar in fluid inclusions of SE Australian xenoliths. Geochem. J. 36, 209–217. https://doi.org/10.2343/geochemj.36.209

Matusiak-Małek, M., Puziewicz, J., Ntaflos, T., Grégoire, M., Kukuła, A., Wojtulek, P.M., 2017. Origin and evolution of rare amphibole-bearing mantle peridotites from Wilcza Góra (SW Poland), Central Europe. Lithos 286–287, 302–323. https://doi.org/10.1016/j.lithos.2017.06.017

McDonough, W.F., Sun, S. -s., 1995. The composition of the Earth. Chem. Geol. 120, 223–253. https://doi.org/10.1016/0009-2541(94)00140-4

Melchiorre, M., Faccini, B., Grégoire, M., Benoit, M., Casetta, F., Coltorti, M., 2020. Melting and metasomatism/refertilisation processes in the Patagonian sub-continental lithospheric mantle: A review. Lithos 354–355, 105324. https://doi.org/10.1016/j.lithos.2019.105324

Mercier, J-C.C., Nicolas, A., 1975. Textures and fabrics of upper-mantle peridotites as illustrated by xenoliths from basalts. J. Petrol. 16, 454–487. https://doi.org/10.1093/petrology/16.1.454

Mertes, H., Schmincke, H.U., 1985. Mafic potassic lavas of the Quaternary West Eifel volcanic field - I. Major and trace elements. Contrib. to Mineral. Petrol. 89, 330–345. https://doi.org/10.1007/BF00381555

Miller, W.G.R., Holland, T.J.B., Gibson, S.A., 2016. Garnet and spinel oxybarometers: New internally consistent multi-equilibria models with applications to the oxidation state of the lithospheric mantle. J. Petrol. 57, 1199–1222. https://doi.org/10.1093/petrology/egw037

Moreira, M., 2013. Noble gas constraints on the origin and evolution of earth's volatiles. Geochemical Perspect. 2, 229–230. https://doi.org/10.7185/geochempersp.2.2

Moreira, M., Kunz, J., Allègre, C., 1998. Rare gas systematics in popping rock: Isotopic and elemental compositions in the upper mantle. Science 279, 1178–1181. https://doi.org/10.1126/science.279.5354.1178

Moreira, M., Rouchon, V., Muller, E., Noirez, S., 2018. The xenon isotopic signature of the mantle beneath Massif Central. Geochemical Perspect. Lett. 6, 28–32. https://doi.org/10.7185/geochemlet.1805

Moreva-Perekalina, T. V, 1985. Ultramafic xenoliths from alkaline basalts of Finkenberg (Siebengebirge, West Germany), in: Scripta Geologica, 78, 1–65. Rijksmuseum van Geologie en Mineralogie.

Mukhopadhyay, S., 2012. Early differentiation and volatile accretion recorded in deep-mantle neon and xenon. Nature 486, 101–104. https://doi.org/10.1038/nature11141

Niu, Y., Langmuir, C.H., Kinzler, R.J., 1997. The origin of abyssal peridotites: A new perspective. Earth Planet. Sci. Lett. 152, 251–265. https://doi.org/10.1016/s0012-821x(97)00119-2

Nowell, D.A.G., Jones, M.C., Pyle, D.M., 2006. Episodic Quaternary volcanism in France and Germany. J. Quat. Sci. 21, 645–675. https://doi.org/10.1002/jqs.1005

Nuccio, P.M., Paonita, A., Rizzo, A., Rosciglione, A., 2008. Elemental and isotope covariation of noble gases in mineral phases from Etnean volcanics erupted during 2001-2005, and genetic relation with peripheral gas discharges. Earth Planet. Sci. Lett. 272, 683–690. https://doi.org/10.1016/j.epsl.2008.06.007

Oppenheimer, C., Moretti, R., Kyle, P.R., Eschenbacher, A., Lowenstern, J.B., Hervig, R.L., Dunbar, N.W., 2011. Mantle to surface degassing of alkalic magmas at Erebus volcano, Antarctica. Earth Planet. Sci. Lett. 306, 261–271. https://doi.org/10.1016/j.epsl.2011.04.005

Ozima, M., Podosek, F.A., 2002. Noble gas geochemistry. Second edition. Cambridge University Press, Cambridge.

Pearce, J.A., Barker, P.F., Edwards, S.J., Parkinson, I.J., Leat, P.T., 2000. Geochemistry and tectonic significance of peridotites from the South Sandwich arc-basin system, South Atlantic. Contrib. to Mineral. Petrol. 139, 36–53. https://doi.org/10.1007/s004100050572

Pouchou, J.-L., Pichoir, F., 1991. Quantitative Analysis of Homogeneous or Stratified Microvolumes Applying the Model “PAP,” in: Heinrich, K.F.J., Newbury, D.E. (Eds.), Electron Probe Quantitation. Springer US, Boston, MA, pp. 31–75. https://doi.org/10.1007/978-1-4899-2617-3_4

Ritter, J.R.R., 2007. The Seismic Signature of the Eifel Plume, in: Ritter, J.R.R., Christensen, U.R. (Eds.), Mantle Plumes. Springer Berlin Heidelberg, Berlin, Heidelberg, pp. 379–404. https://doi.org/10.1007/978-3-540-68046-8_12

Ritter, J.R.R., Jordan, M., Christensen, U.R., Achauer, U., 2001. A mantle plume below the Eifel volcanic fields, Germany. Earth Planet. Sci. Lett. 186, 7–14. https://doi.org/10.1016/S0012-821X(01)00226-6

Rizzo, A.L., Barberi, F., Carapezza, M.L., Di Piazza, A., Francalanci, L., Sortino, F., D’Alessandro, W., 2015. New mafic magma refilling a quiescent volcano: Evidence from He-Ne-Ar isotopes during the 2011-2012 unrest at Santorini, Greece. Geochemistry, Geophys. Geosystems 16, 798–814. https://doi.org/10.1002/2014GC005653

Rizzo, A.L., Pelorosso, B., Coltorti, M., Ntaflos, T., Bonadiman, C., Matusiak-Małek, M., Italiano, F., Bergonzoni, G., 2018. Geochemistry of noble gases and CO_2 in fluid inclusions from lithospheric mantle beneath wilcza góra (Lower silesia, southwest Poland). Front. Earth Sci. 6, 215. https://doi.org/10.3389/feart.2018.00215

Roedder, E., 1984. Fluid inclusions, Reviews in Mineralogy, Vol. 12. Mineralogical Society of America.

Sarda, P., 2004. Surface noble gas recycling to the terrestrial mantle. Earth Planet. Sci. Lett. 228, 49–63.

https://doi.org/10.1016/j.epsl.2004.09.026
Sarda, P., Staudacher, T., Allègre, C.J., 1988. Neon isotopes in submarine basalts. Earth Planet. Sci. Lett. 91, 73–88. https://doi.org/10.1016/0012-821X(88)90152-5
Schmincke, H.-U., 2007. The Quaternary Volcanic Fields of the East and West Eifel (Germany), in: Ritter, J.R.R., Christensen, U.R. (Eds.), Mantle Plumes. Springer Berlin Heidelberg, Berlin, Heidelberg, pp. 241–322. https://doi.org/10.1007/978-3-540-68046-8_8
Schmincke, H.-U., Lorenz, V., Seck, H.A., 1983. The Quaternary Eifel Volcanic Fields, in: Fuchs, K., von Gehlen, K., Mälzer, H., Murawski, H., Semmel, A. (Eds.), Plateau Uplift. Springer Berlin Heidelberg, Berlin, Heidelberg, pp. 139–151. https://doi.org/10.1007/978-3-642-69219-2_21
Shaw, C.S.J., Eyzaguirre, J., Fryer, B., Gagnon, J., 2005. Regional variations in the mineralogy of metasomatic assemblages in mantle xenoliths from the West Eifel Volcanic Field, Germany. J. Petrol. 46, 945–972. https://doi.org/10.1093/petrology/egi006
Shaw, C.S.J., Lebert, B.S., B.Woodland, A., 2018. Thermodynamic modelling of mantle-melt interaction evidenced by veined wehrlite xenoliths from the Rockeskyllerkopf Volcanic Complex, west eifel volcanic field, Germany. J. Petrol. 59, 59–86. https://doi.org/10.1093/petrology/egy018
Stachel, T., Luth, R.W., 2015. Diamond formation - Where, when and how? Lithos 220–223, 200–220. https://doi.org/10.1016/j.lithos.2015.01.028
Stosch, H.G., Lugmair, G.W., 1986. Trace element and Sr and Nd isotope geochemistry of peridotite xenoliths from the Eifel (West Germany) and their bearing on the evolution of the subcontinental lithosphere. Earth Planet. Sci. Lett. 80, 281–298. https://doi.org/10.1016/0012-821X(86)90111-1
Stosch, H.G., Seck, H.A., 1980. Geochemistry and mineralogy of two spinel peridotite suites from Dreiser Weiher, West Germany. Geochim. Cosmochim. Acta 44, 457–470. https://doi.org/10.1016/0016-7037(80)90044-7
Sun, S. -s., McDonough, W.F., 1989. Chemical and isotopic systematics of oceanic basalts: implications for mantle composition and processes. Geol. Soc. London, Spec. Publ. 42, 313–345. https://doi.org/10.1144/GSL.SP.1989.042.01.19
Todt, W., Lippolt, H.J., 1980. K-Ar age determinations on Tertiary volcanic rocks: V. Siebengebirge, Siebengebirge- Graben. J. Geophys. 48, 18–27.
Trieloff, M., Altherr, R., 2007. He-Ne-Ar Isotope Systematics of Eifel and Pannonian Basin Mantle Xenoliths Trace Deep Mantle Plume-Lithosphere Interaction Beneath the European Continent, in: Ritter, J.R.R., Christensen, U.R. (Eds.), Mantle Plumes. Springer Berlin Heidelberg, Berlin, Heidelberg, pp. 339–367. https://doi.org/10.1007/978-3-540-68046-8_10
Trull, T.W., Kurz, M.D., 1993. Experimental measurements of ^{3}He and ^{4}He mobility in olivine and clinopyroxene at magmatic temperatures. Geochim. Cosmochim. Acta 57, 1313–1324.

https://doi.org/10.1016/0016-7037(93)90068-8

Upton, B.G.J., Downes, H., Kirstein, L.A., Bonadiman, C., Hill, P.G., Ntaflos, T., 2011. The lithospheric mantle and lower crust–mantle relationships under Scotland: a xenolithic perspective. J. Geol. Soc. London. 168, 873–886. https://doi.org/10.1144/0016-76492009-172

Valbracht, P.J., Honda, M., Matsumoto, T., Mattielli, N., McDougall, I., Ragettli, R., Weis, D., 1996. Helium, neon and argon isotope systematics in Kerguelen ultramafic xenoliths: Implications for mantle source signatures. Earth Planet. Sci. Lett. 138, 29–38. https://doi.org/10.1016/0012-821x(95)00226-3

Vieten, K., Hamm, H.M., Grimmeisen, W., 1988. Tertiärer vulkanismus des Siebengebirges. Fortschritte der Mineral. 66, 1–39.

Weinlich, F.H., Bräuer, K., Kämpf, H., Strauch, G., Tesař, J., Weise, S.M., 1999. An active subcontinental mantle volatile system in the western Eger rift, Central Europe: gas flux, isotopic (He, C, and N) and compositional fingerprints. Geochim. Cosmochim. Acta 63, 3653–3671. https://doi.org/10.1016/S0016-7037(99)00187-8

Wilson, M., Downes, H., 2006. Tertiary-Quaternary intra-plate magmatism in Europe and its relationship to mantle dynamics, in: Gee, D.G., Stephenson, R.A. (Eds.), European Lithosphere Dynamics, Geol. Soc. London Memoirs, 32, 147–166. https://doi.org/10.1144/GSL.MEM.2006.032.01.09

Wilson, M., Downes, H., 1991. Tertiary - quaternary extension-related alkaline magmatism in Western and central Europe. J. Petrol. 32, 811–849. https://doi.org/10.1093/petrology/32.4.811

Witt-Eickschen, G., 2007. Thermal and Geochemical Evolution of the Shallow Subcontinental Lithospheric Mantle Beneath the Eifel: Constraints from Mantle Xenoliths, a Review, in: Ritter, J.R.R., Christensen, U.R. (Eds.), Mantle Plumes. Springer Berlin Heidelberg, Berlin, Heidelberg, pp. 323–337. https://doi.org/10.1007/978-3-540-68046-8_9

Witt-Eickschen, G., Harte, B., 1994. Distribution of trace elements between amphibole and clinopyroxene from mantle peridotites of the Eifel (western Germany): An ion-microprobe study. Chem. Geol. 117, 235–250. https://doi.org/10.1016/0009-2541(94)90130-9

Witt-Eickschen, G., Kaminsky, W., Kramm, U., Harte, B., 1998. The nature of young vein metasomatism in the lithosphere of the West Eifel (Germany): Geochemical and isotopic constraints from composite mantle xenoliths from the meerfelder maar. J. Petrol. 39, 155–185. https://doi.org/10.1093/petroj/39.1.155

Witt-Eickschen, G., Kramm, U., 1998. Evidence for the multiple stage evolution of the subcontinental lithospheric mantle beneath the Eifel (Germany) from pyroxenite and composite pyroxenite/peridotite xenoliths. Contrib. to Mineral. Petrol. 131, 258–272. https://doi.org/10.1007/s004100050392

Witt-Eickschen, G., O'Neill, H.S.C., 2005. The effect of temperature on the equilibrium distribution of trace elements between clinopyroxene, orthopyroxene, olivine and spinel in upper mantle peridotite. Chem. Geol. 221, 65–101. https://doi.org/10.1016/j.chemgeo.2005.04.005

Witt-Eickschen, G., Seck, H.A., Mezger, K., Eggins, S.M., Altherr, R., 2003. Lithospheric mantle evolution beneath the Eifel (Germany): Constraints from Sr-Nd-Pb isotopes and trace element abundances in spinel peridotite and pyroxenite xenoliths. J. Petrol. 44, 1077–1095. https://doi.org/10.1093/petrology/44.6.1077

Witt-Eickschen, G., Seck, H.A., Reys, C., 1993. Multiple Enrichment Processes and their Relationships in the Subcrustal Lithosphere Beneath the Eifel (Germany). J. Petrol. 34, 1–22. https://doi.org/10.1093/petrology/34.1.1

Witt, G., Seck, H.A., 1989. Origin of amphibole in recrystallized and porphyroclastic mantle xenoliths from the Rhenish Massif: implications for the nature of mantle metasomatism. Earth Planet. Sci. Lett. 91, 327–340. https://doi.org/10.1016/0012-821X(89)90007-1

Witt, G., Seck, H.A., 1987. Temperature history of sheared mantle xenoliths from the West Eifel, West Germany: Evidence for mantle diapirism beneath the rhenish massif. J. Petrol. 28, 475–493. https://doi.org/10.1093/petrology/28.3.475

Woodland, A.B., Kornprobst, J., McPherson, E., Bodinier, J.L., Menzies, M.A., 1996. Metasomatic interactions in the lithospheric mantle: Petrologic evidence from the Lherz massif, French Pyrenees. Chem. Geol. 134, 83–112. https://doi.org/10.1016/S0009-2541(96)00082-4

Woodland, A.B., Kornprobst, J., Tabit, A., 2006. Ferric iron in orogenic lherzolite massifs and controls of oxygen fugacity in the upper mantle. Lithos 89, 222–241. https://doi.org/10.1016/j.lithos.2005.12.014

Yamamoto, J., Kaneoka, I., Nakai, S., Kagi, H., Prikhod’ko, V.S., Arai, S., 2004. Evidence for subduction-related components in the subcontinental mantle from low $^{3}He/^{4}He$ and $^{40}Ar/^{36}Ar$ ratio in mantle xenoliths from Far Eastern Russia. Chem. Geol. 207, 237–259. https://doi.org/10.1016/j.chemgeo.2004.03.007

Yamamoto, J., Nishimura, K., Sugimoto, T., Takemura, K., Takahata, N., Sano, Y., 2009. Diffusive fractionation of noble gases in mantle with magma channels: Origin of low He/Ar in mantle-derived rocks. Earth Planet. Sci. Lett. 280, 167–174. https://doi.org/10.1016/j.epsl.2009.01.029

Ziegler, P.A., 1992. European Cenozoic rift system. Tectonophysics 208, 91–111. https://doi.org/10.1016/0040-1951(92)90338-7

Ziegler, P.A., Schumacher, M.E., Dèzes, P., Van Wees, J.-D., Cloetingh, S., 2004. Post-Variscan evolution of the lithosphere in the Rhine Graben area: constraints from subsidence modelling. Geol. Soc. London, Spec. Publ. 223, 289–317. https://doi.org/10.1144/GSL.SP.2004.223.01.13

Zolitschka, B., Negendank, J.F.W., Lottermoser, B.G., 1995. Sedimentological proof and dating of the Early Holocene volcanic eruption of Ulmener Maar (Vulkaneifel, Germany). Geol. Rundschau 84, 213–219. https://doi.org/10.1007/BF00192252

Figure captions

Figure 1. a) Map of Rhine rift system from Ziegler et al. (2004), showing Cenozoic fault systems (black lines), rift-related sedimentary basins (light grey), outcropping parts of the Variscan orogen (dark grey) and Cenozoic volcanic fields (black). b) Enlargement of part of figure 1a, modified from Schmincke et al. (1983), showing Cenozoic volcanic fields on the uplifted Rhenish shield and in adjacent areas. The area of the Eocene Hocheifel Volcanic Field (HEVF) overlaps that of the Quaternary West and East Eifel Volcanic Fields (WEVF and EEVF). c) Google Earth map showing the sampling sites location in West Eifel (Dreiser Weiher, Gees and Meerfelder Maar) and Siebengebirge (Willmeroth and Eulenberg) volcanic fields. d) Neck made of columnar basalts located on the eastern side of Rheine River, within the Siebengebirge volcanic area. e) Ultramafic xenoliths embedded within massive lava flows, sills and/or necks, as typically occurs in Siebengebirge volcanic field. f) Ultramafic xenoliths found within scoria cone, pyroclastic deposits and/or within maars, as typically occurs in West Eifel volcanic field.

Figure 2. Olivine (Ol) - orthopyroxene (Opx) - clinopyroxene (Cpx) ternary diagrams showing the composition of ultramafic xenoliths from a) West Eifel and b) Siebengebirge. Primitive mantle (PM) composition is from Johnson et al. (1990). Melting trends at 1 GPa and 0 to 1 wt% H_2O and at 2 GPa and 0 wt% H_2O (from Bénard et al., 2018 and Niu et al., 1997) are also shown for comparison.

Figure 3. Forsterite (Fo) vs. NiO (wt%) content of olivine in West Eifel and Siebengebirge ultramafic xenoliths. Black square indicates the olivine composition in Primordial Mantle (PM) calculated through mass balance from Bulk Silicate Earth of McDonough and Sun (1995) and Johnson et al. (1990) modes. The compositional field of olivine from West Eifel ultramafic xenoliths reported in literature (Ban et al., 2005; Lloyd et al., 1991; Shaw et al., 2018; Witt-Eickschen et al., 1993; Witt-Eickschen and O'Neill, 2005) is also plotted for comparison. Ol = olivine; Amph = amphibole; Phl = phlogopite.

Figure 4. Major element composition of pyroxene in West Eifel and Siebengebirge ultramafic xenoliths. a) Mg# vs. Al_2O_3 and b) Mg# vs. TiO_2 diagrams showing the composition of clinopyroxene; c) Mg# vs. Al_2O_3 and d) Mg# vs. TiO_2 diagrams showing the composition of orthopyroxene. Dashed vertical lines represent the Mg# thresholds used to discriminate between cumulates and mantle clinopyroxene and orthopyroxene. The composition of clinopyroxene and orthopyroxene in West Eifel ultramafic xenoliths from previous studies (Ban et al., 2005; Lloyd et al., 1991; Shaw et al., 2018; Stosch and Lugmair, 1986; Witt-Eickschen

et al., 2003, 1998, 1993; Witt-Eickschen and Harte, 1994; Witt-Eickschen and O'Neill, 2005) is also reported for comparison. Ol = olivine; Amph = amphibole; Phl = phlogopite.

Figure 5. Olivine-spinel mantle array (OSMA) diagram (Arai, 1994) showing the composition of olivine and spinel in West Eifel and Siebengebirge ultramafic xenoliths. Primordial Mantle (PM) composition of olivine and spinel was calculated through mass balance from Bulk Silicate Earth of McDonough and Sun (1995) and Johnson et al. (1990) modes. Compositional fields of Supra-Subduction Zone (SSZ; Pearce et al., 2000) and Abyssal Peridotites (Dick and Bullen, 1984) are also shown for comparison. Ol = olivine; Amph = amphibole; Phl = phlogopite.

Figure 6. a) Temperature (T; °C) vs. oxygen fugacity ($\Delta \log fO_2$ [FMQ]) diagram showing the equilibrium conditions recorded by the studied ultramafic xenoliths. Equilibrium temperatures were calculated with the olivine-spinel exchange thermometer of Ballhaus et al. (1991). Oxygen fugacity was calculated with the olivine-spinel-orthopyroxene oxybarometer of Miller et al. (2016). For each sample, average values are reported, and error bars indicate the standard deviation of the results. b) Al_2O_3 (wt%) vs. MgO (wt%) in clinopyroxene and c) Al_2O_3 (wt%) vs. MgO (wt%) in orthopyroxene in West Eifel and Siebengebirge ultramafic xenoliths. The melting curves reported in b) and c) refer to the melting model of Bonadiman and Coltorti (2011) and Upton et al. (2011), developed from a starting Primitive mantle (PM) composition (Sun and McDonough, 1989). The composition of clinopyroxene and orthopyroxene in West Eifel ultramafic xenoliths from previous studies (Ban et al., 2005; Lloyd et al., 1991; Shaw et al., 2018; Stosch and Lugmair, 1986; Witt-Eickschen et al., 2003, 1998, 1993; Witt-Eickschen and Harte, 1994; Witt-Eickschen and O'Neill, 2005) is also reported for comparison. Ol = olivine; Amph = amphibole; Phl = phlogopite.

Figure 7. Elemental concentrations in mol/g of ^{4}He vs. a) $^{40}Ar^*$, b) CO_2, c) N_2^*; and d) $^{21}Ne^*$ measured in fluid inclusions from West Eifel and Siebengebirge xenoliths after single-step crushing. Available data from other European mantle xenoliths localities are also reported for comparison [French Massif Central, Eifel, and Kapfenstein (Gautheron et al., 2005); Calatrava and Tallante (Martelli et al., 2011); Lower Silesia (Rizzo et al., 2018); Persani Mts (PMVF; Faccini et al., 2020)]. Solid and dashed lines in a) represent $^{4}He/^{40}Ar$ ratios of 0.05 and 5, respectively. Solid and dashed lines in b) represent $^{4}He/CO_2$ ratios of 10^{-4} and 10^{-6}, respectively. MM = Meerfelder Maar; DBR = Dreiser Weiher; GE = Gees; SB = Willmeroth; EUL = Eulenberg. Amph = amphibole; Phl = phlogopite.

Figure 8. Concentration of a) ^{4}He (mol/g) and b) ^{3}He (mol/g) vs. Rc/Ra ($^{3}He/^{4}He$ corrected for air contamination) measured in fluid inclusions from West Eifel and Siebengebirge xenoliths after single-step

crushing. The light blue field indicates the range of $^3He/^4He$ ratios for a MORB-like mantle (8±1 Ra; Graham, 2002). The violet field indicates the range of $^3He/^4He$ ratios measured in East Eifel surface gases (Aeschbach-Hertig et al., 1996; Bräuer et al., 2013, 2005; Giggenbach et al., 1991; Griesshaber et al., 1992). The two diffusive fractionation paths (red solid and dashed lines) are modeled based on the approach of Burnard et al. (1998), Burnard (2004) and Yamamoto et al. (2009), taking into account the diffusion coefficient (D) of ^3He, ^4He, and $^{40}Ar^*$ (D_{3He}/D_{4He} = 1.15 and D_{4He}/D_{40Ar} = 3.16 in solid mantle; Burnard, 2004; Trull and Kurz, 1993; Yamamoto et al., 2009). Starting mantle composition is: $^4He = 2.5\times10^{-13}$ mol/g, $^3He = 2.1\times10^{-18}$ mol/g, $^{40}Ar^* = 8.3\times10^{-14}$ mol/g, and $^3He/^4He$ = 6.0 Ra. These values were chosen considering the decrease of $^3He/^4He$ noticed in most of the European samples and a $^4He/^{40}Ar^*$ ratio within the reported range for mantle production ($^4He/^{40}Ar^*$ = 1-5; Marty, 2012) (see also Faccini et al., 2020). Symbols as in Figure 7.

Figure 9. Concentrations of a) $^{21}Ne/^{22}Ne$ vs. $^{20}Ne/^{22}Ne$ and b) $^3He/^{36}Ar$ vs. $^{40}Ar/^{36}Ar$ measured in fluid inclusions from West Eifel and Siebengebirge xenoliths after single-step crushing. In a), the black solid to dashed lines represent binary mixing between air ($^{21}Ne/^{22}Ne$ = 0.0290 and $^{20}Ne/^{22}Ne$ = 9.8) and i) MORB-like mantle [$^{21}Ne/^{22}Ne$ = 0.06 and $^{20}Ne/^{22}Ne$ = 12.5 (Sarda et al. 1988; Moreira et al. 1998)], ii) CRUST [$^{21}Ne/^{22}Ne$ = 0.6145 (mean of 0.469-0.76) and $^{20}Ne/^{22}Ne$ = 0.3 (Ballentine, 1997 and references therein) and iii) Solar Wind [$^{21}Ne/^{22}Ne$ = 0.0328 and $^{20}Ne/^{22}Ne$ = 13.8 (Heber et al., 2009)]. In b), the black solid to dashed lines represent binary mixing between air [$^{40}Ar/^{36}Ar$ = 295.5, $^3He/^{36}Ar = 2.3\times10^{-7}$ and $^4He = 1.1\times10^{-16}$ (arbitrarily fixed to fit data) (Ozima and Podosek, 2002)] and MORB-like mantle [$^{40}Ar/^{36}Ar$ = 44,000, $^3He/^{36}Ar$ = 2.45 and 0.0245 and $^4He = 1.0\times10^{-9}$ (arbitrarily fixed to fit data), considering $^3He/^4He$ = 8, $^4He/^{40}Ar^*$ = 5 and $^4He/^{40}Ar^*$ = 0.05 (see Ballentine et al., 2005; Moreira et al., 1998)]. Symbols as in Figure 7.

Figure 10. $^4He/^{40}Ar^*$ vs. Rc/Ra ($^3He/^4He$ corrected for air contamination) measured in fluid inclusions from West Eifel and Siebengebirge xenoliths after single-step crushing. The light blue field represents the MORB-like ranges of $^3He/^4He$ (8±1 Rc/Ra; Graham, 2002) and the $^4He/^{40}Ar^*$ mantle production ratio (1-5; Marty, 2012). The two diffusive fractionation paths (red solid and dashed lines) are modeled as explained in the caption of Figure 8, from a starting mantle composition (black square) having $^3He/^4He$ = 6.0 Ra and a $^4He/^{40}Ar^*$ ratio within the reported range for mantle production ($^4He/^{40}Ar^*$ = 1-5; Marty, 2012) (see also Faccini et al., 2020). Arrows indicate the main $^3He/^4He$ and $^4He/^{40}Ar^*$ behaviour during refertilization, partial melting and assimilation of crustal components. Available data from other European mantle xenoliths localities are also reported for comparison as in Figure 7. MM = Meerfelder Maar; DBR = Dreiser Weiher; GE = Gees; SB = Willmeroth; EUL = Eulenberg. Amph = amphibole; Phl = phlogopite.

Figure 11. Mg# vs. a) $^4He/^{40}Ar^*$, and b) Rc/Ra ($^3He/^4He$ corrected for air contamination) diagrams showing the composition of West Eifel and Siebengebirge ultramafic xenoliths. The light blue field represents the MORB-like ranges of $^3He/^4He$ (8±1 Rc/Ra; Graham, 2002)and $^4He/^{40}Ar^*$ (1-5; Marty, 2012). Arrows indicate the excepted trends during refertilization, partial melting and assimilation of crustal components. The vertical dotted line indicates the typical Mg# threshold between cumulates and mantle lithotypes. The violet field in b) indicates the $^3He/^4He$ range measured in East Eifel surface gases (Aeschbach-Hertig et al., 1996; Bräuer et al., 2013, 2005; Giggenbach et al., 1991; Griesshaber et al., 1992). Symbols as in Figg. 7 and 10.

Figure 12. Relationships between equilibrium temperature (T; °C) recorded by West Eifel and Siebengebirge ultramafic xenoliths and a) Al_2O_3 (wt%) content of pyroxene; b) Rc/Ra ($^3He/^4He$ corrected for air contamination) ratio measured in the main phase constituents (olivine, orthopyroxene, clinopyroxene). Note the positive correlation between equilibrium T and Al_2O_3 (wt%) content of pyroxene in panel a), and the concomitant negative correlation between T and Rc/Ra content in panel b). Ol = olivine; Amph = amphibole; Phl = phlogopite.

Supplementary Figures

Figure S1. High resolution thin section scans of representative ultramafic xenoliths from West Eifel and Siebengebirge (see text for further explanation). a) Fine-grained protogranular to tabular equigranular amphibole-bearing harzburgite from Meerfelder Maar (sample MM5); b) Protogranular, slightly foliated anhydrous lherzolite from Meerfelder Maar (sample MM7); c) Protogranular anhydrous lherzolite from Dreiser Weiher (sample DBR5); d) Coarse-grained anhydrous olivine-clinopyroxenite with orthocumulitic texture from Dreiser Weiher (sample DBR11); e) Anhydrous olivine-websterite with orthocumulitic texture from Gees (sample GE1); f) Porphyroclastic anhydrous harzburgite from Gees (sample GE3); g) Fine-grained phlogopite-bearing wehrlite from Gees (sample GE5); h) Porphyroclastic anhydrous harzburgite from Eulenberg (sample EUL5); i) Porphyroclastic anhydrous harzburgite from Willmeroth (sample SB5); j) Porphyroclastic anhydrous lherzolite from Willmeroth (sample SB6).

Figure S2. Photomicrographs showing the most representative types and/or associations of FI in the studied West Eifel and Siebengebirge ultramafic xenoliths. a) Isolated FI in clinopyroxene in Meerfelder Maar lherzolite; b) FI trails developed across olivine and clinopyroxene crystals in Meerfelder Maar amphibole-phlogopite-bearing lherzolite; c) FI trail developed in proximity of fractures in a large clinopyroxene grain in Dreiser Weiher wehrlite; d) Cluster of FI hosted in orthopyroxene grain in Dreiser Weiher lherzolite; e) FI trails across orthopyroxene in Gees olivine-websterite; f) and g) FI trails in olivine in Willmeroth dunites;

h) Cross-cutting FI trails hosted in olivine in Willmeroth harzburgite. Ol = olivine; Opx = orthopyroxene; Cpx = clinopyroxene. a), b) and f) = plane-polarized light; c), d), e), g) and h) = cross-polarized light.

Figure S3. Mg# versus a) ^{4}He, b) $^{40}Ar^*$, c) CO_2, and d) N_2^* diagrams showing the composition of West Eifel and Siebengebirge ultramafic xenoliths. The vertical dotted line indicates the typical Mg# threshold between cumulates and mantle lithotypes. Available data from other European mantle xenoliths localities are also reported for comparison [Calatrava and Tallante (Martelli et al., 2011); Lower Silesia (Rizzo et al., 2018); Persani Mts (PMVF; Faccini et al., 2020)]. MM = Meerfelder Maar; DBR = Dreiser Weiher; GE = Gees; SB = Willmeroth; EUL = Eulenberg. Amph = amphibole; Phl = phlogopite.

Figure 1

Click here to access/download;Figure;Figure 1.tif

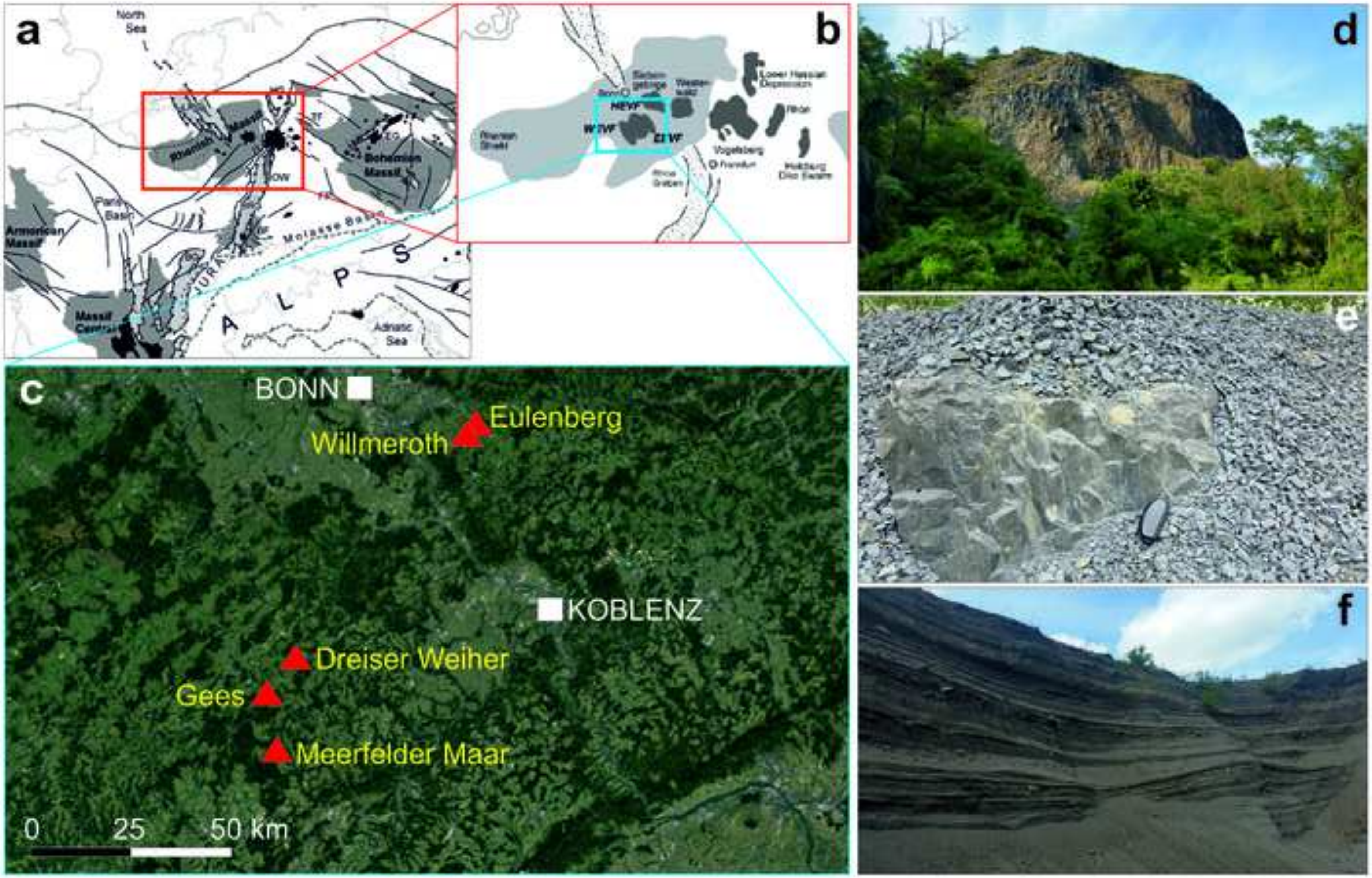

Figure 2

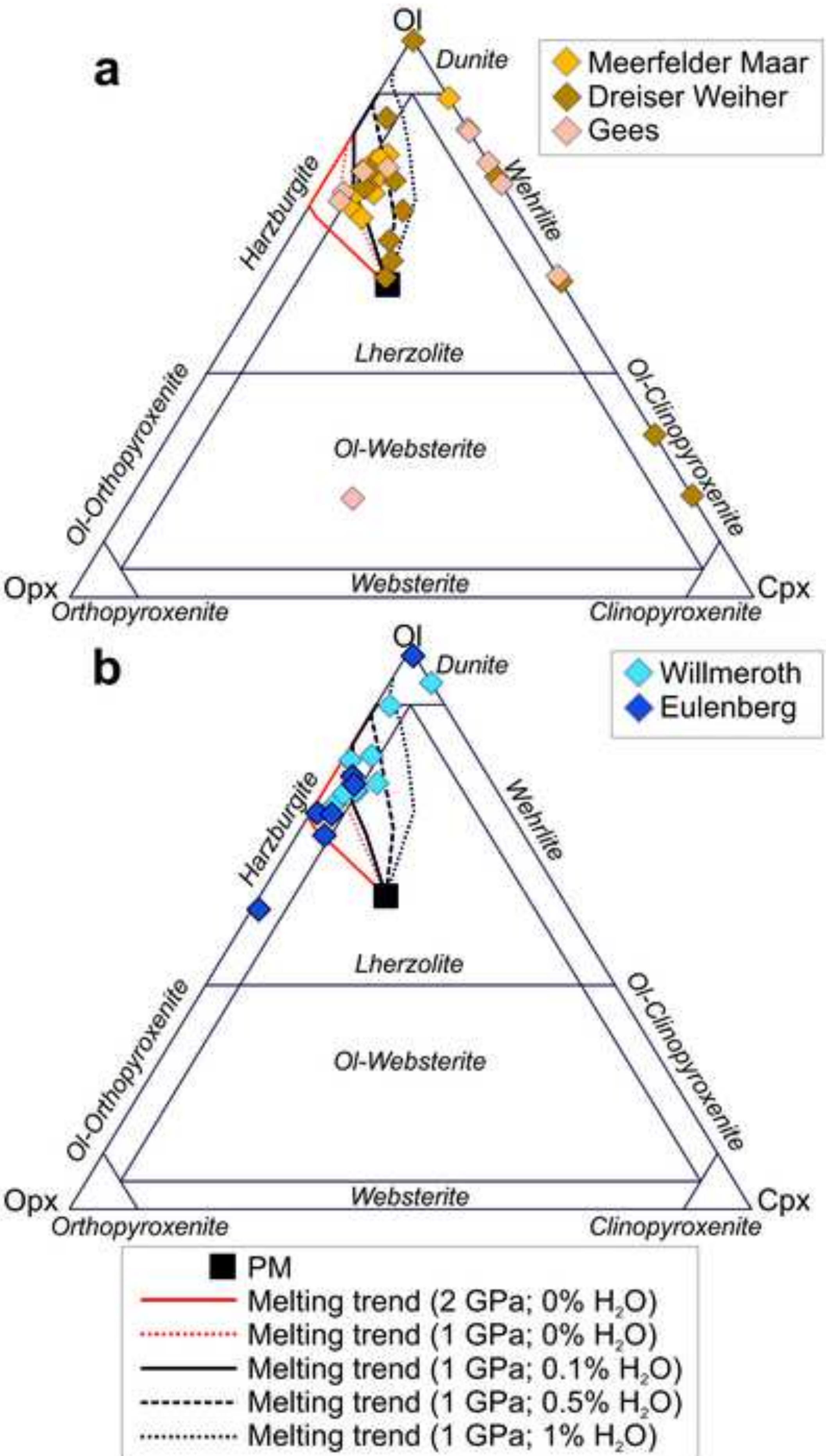
a
Ol
Dunite
Meerfelder Maar
Dreiser Weiher
Gees
Harzburgite
Wehrlite
Lherzolite
Ol-Orthopyroxenite
Ol-Clinopyroxenite
Ol-Websterite
Opx
Websterite
Cpx
Orthopyroxenite
Clinopyroxenite
b
Ol
Dunite
Willmeroth
Eulenberg
Harzburgite
Wehrlite
Lherzolite
Ol-Orthopyroxenite
Ol-Clinopyroxenite
Ol-Websterite
Opx
Websterite
Cpx
Orthopyroxenite
Clinopyroxenite
PM
Melting trend (2 GPa; 0% H_2O)
Melting trend (1 GPa; 0% H_2O)
Melting trend (1 GPa; 0.1% H_2O)
Melting trend (1 GPa; 0.5% H_2O)
Melting trend (1 GPa; 1% H_2O)

Figure 3

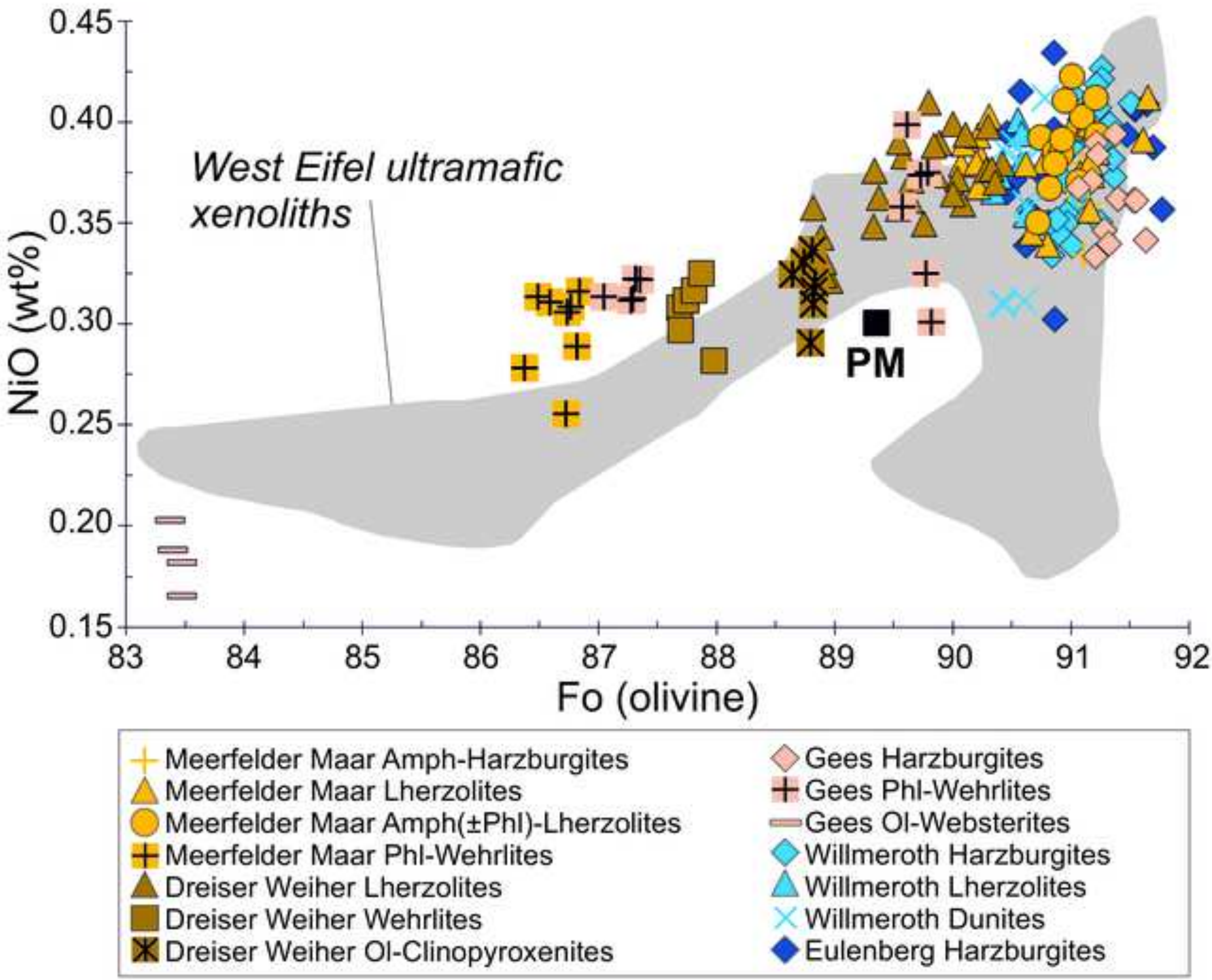

0.45
0.40
0.35
0.30
0.25
0.20
0.15
NiO (wt%)
83
84
85
86
87
88
89
90
91
92
Fo (olivine)
West Eifel ultramafic xenoliths
PM
Meerfelder Maar Amph-Harzburgites
Meerfelder Maar Lherzolites
Meerfelder Maar Amph(±Phl)-Lherzolites
Meerfelder Maar Phl-Wehrlites
Dreiser Weiher Lherzolites
Dreiser Weiher Wehrlites
Dreiser Weiher Ol-Clinopyroxenites
Gees Harzburgites
Gees Phl-Wehrlites
Gees Ol-Websterites
Willmeroth Harzburgites
Willmeroth Lherzolites
Willmeroth Dunites
Eulenberg Harzburgites

Figure 4 Click here to access/download;Figure;Figure 4.tif

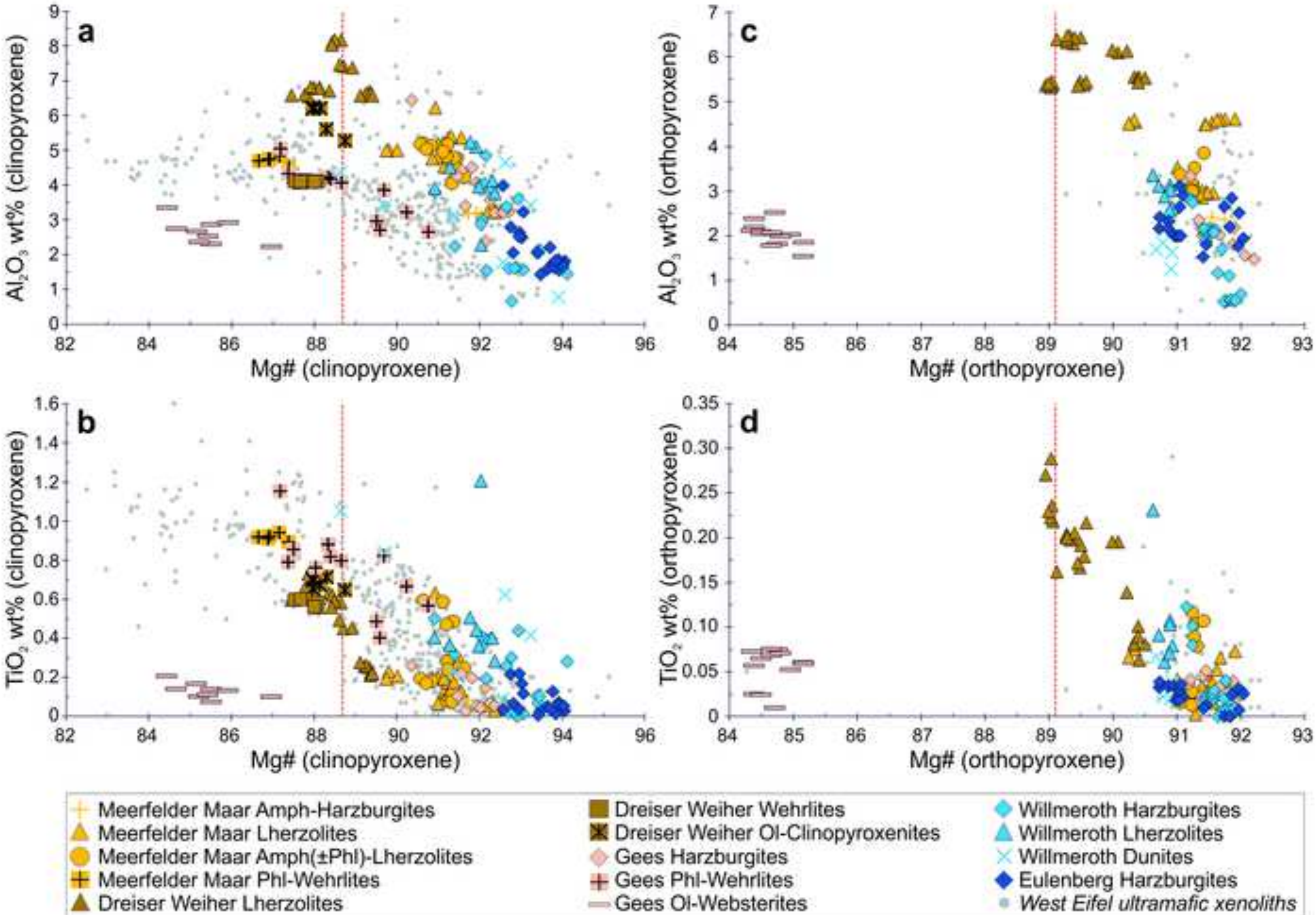

Figure 5

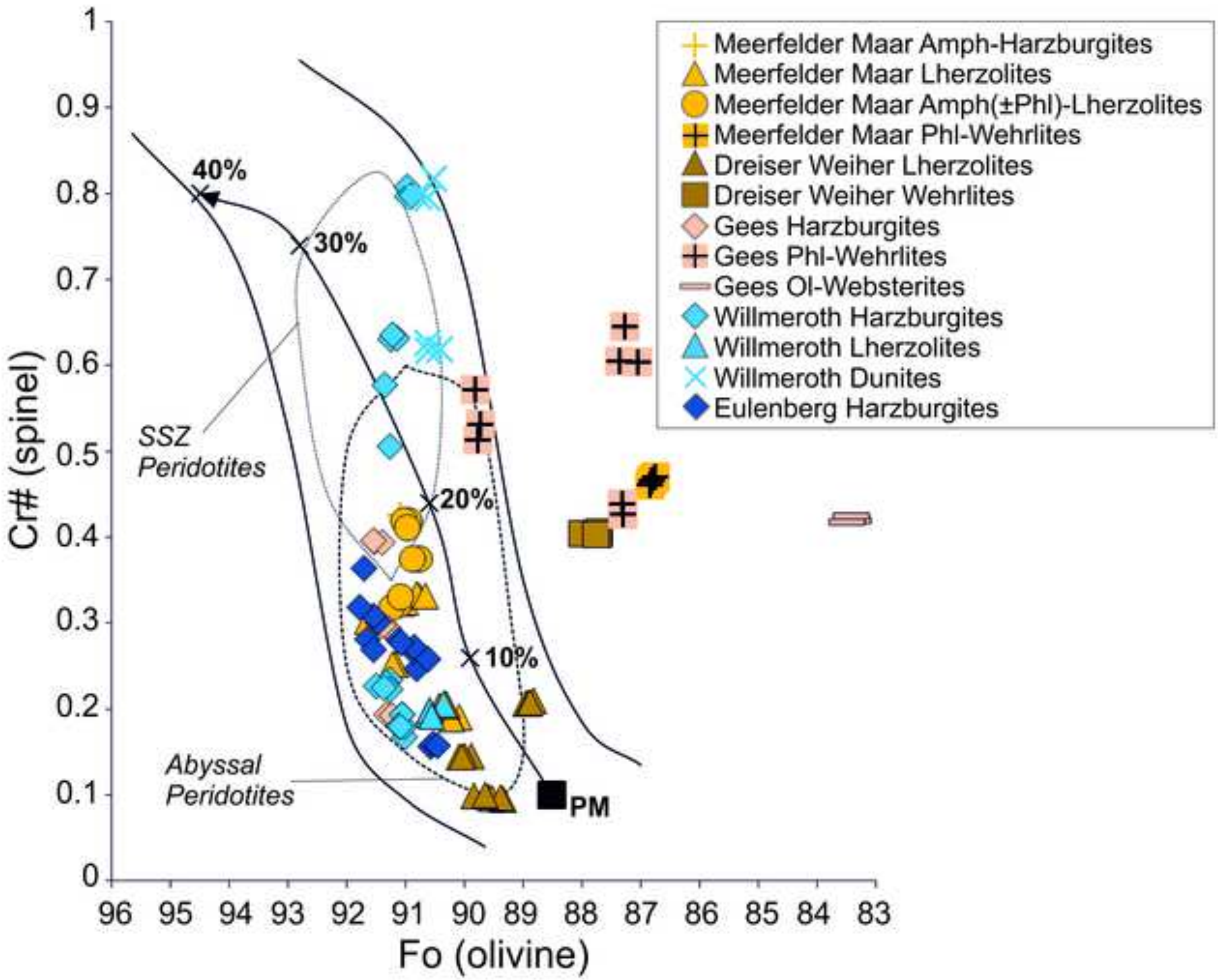
Meerfelder Maar Amph-Harzburgites
Meerfelder Maar Lherzolites
Meerfelder Maar Amph(±Phl)-Lherzolites
Meerfelder Maar Phl-Wehrlites
Dreiser Weiher Lherzolites
Dreiser Weiher Wehrlites
Gees Harzburgites
Gees Phl-Wehrlites
Gees Ol-Websterites
Willmeroth Harzburgites
Willmeroth Lherzolites
Willmeroth Dunites
Eulenberg Harzburgites
40%
30%
20%
10%
PM
SSZ Peridotites
Abyssal Peridotites
Cr# (spinel)
Fo (olivine)
1
0.9
0.8
0.7
0.6
0.5
0.4
0.3
0.2
0.1
0
96
95
94
93
92
91
90
89
88
87
86
85
84
83

Figure 6

Click here to access/download;Figure;Figure 6.tif

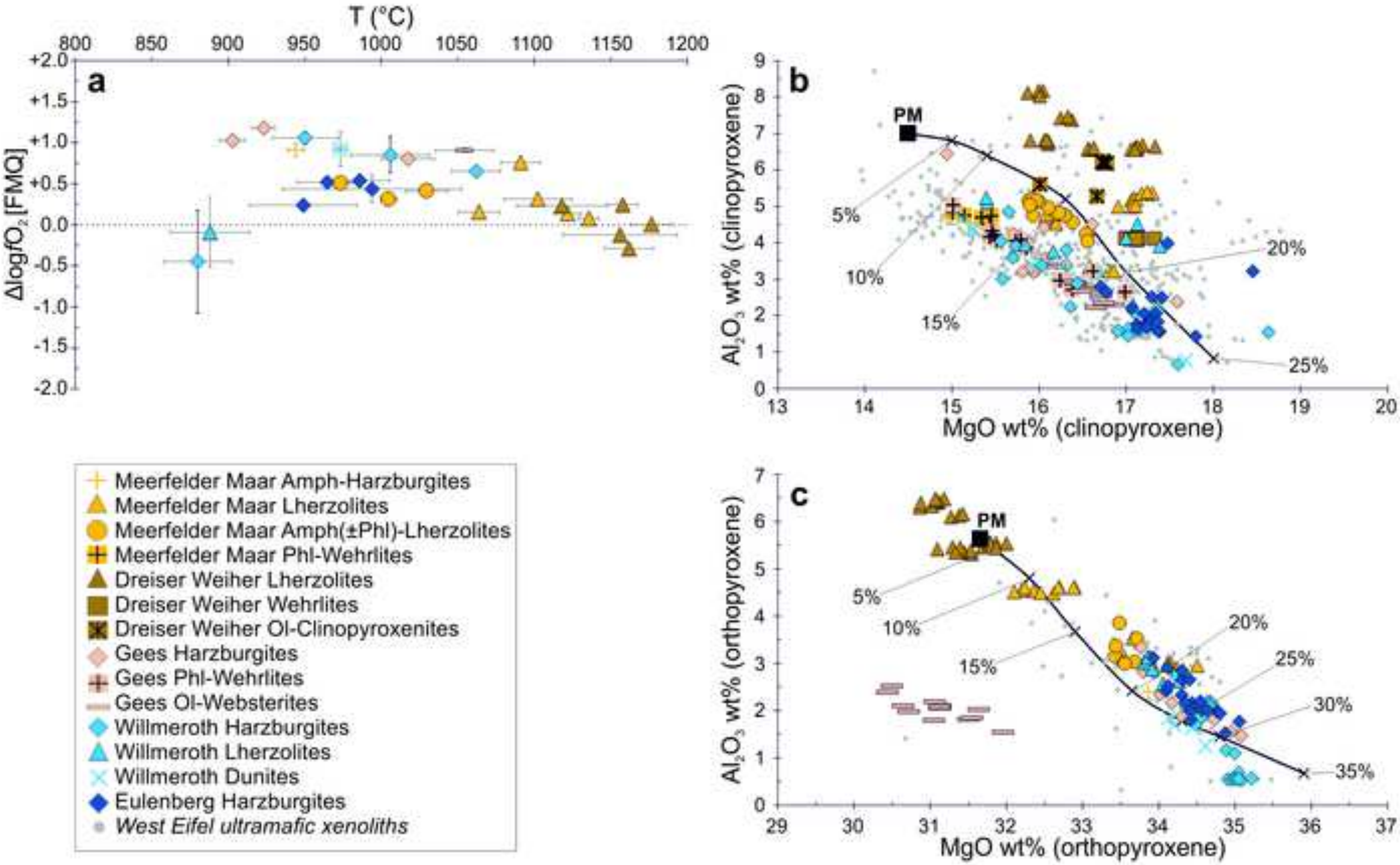

Figure 7

Click here to access/download;Figure;Figure 7.tif

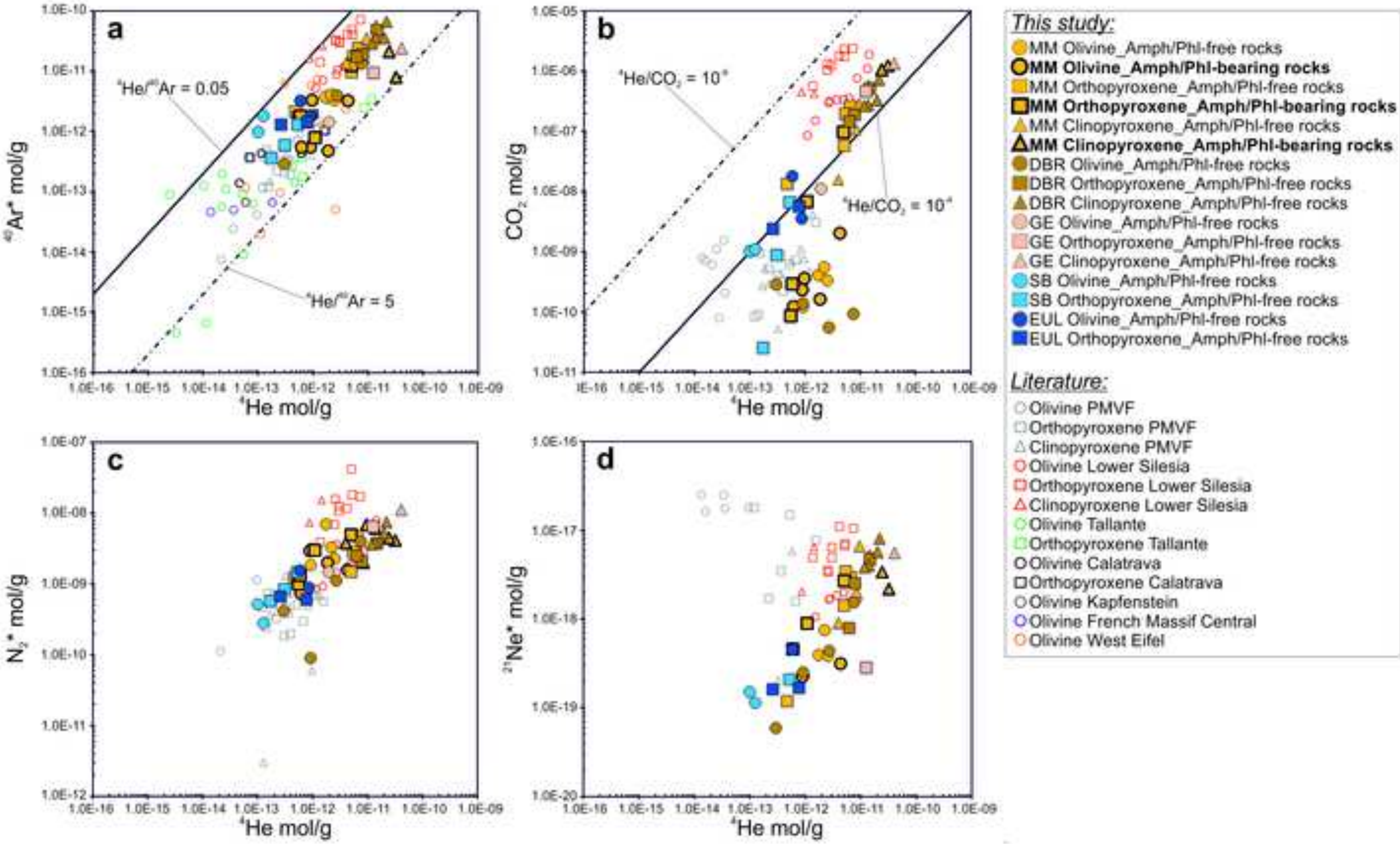

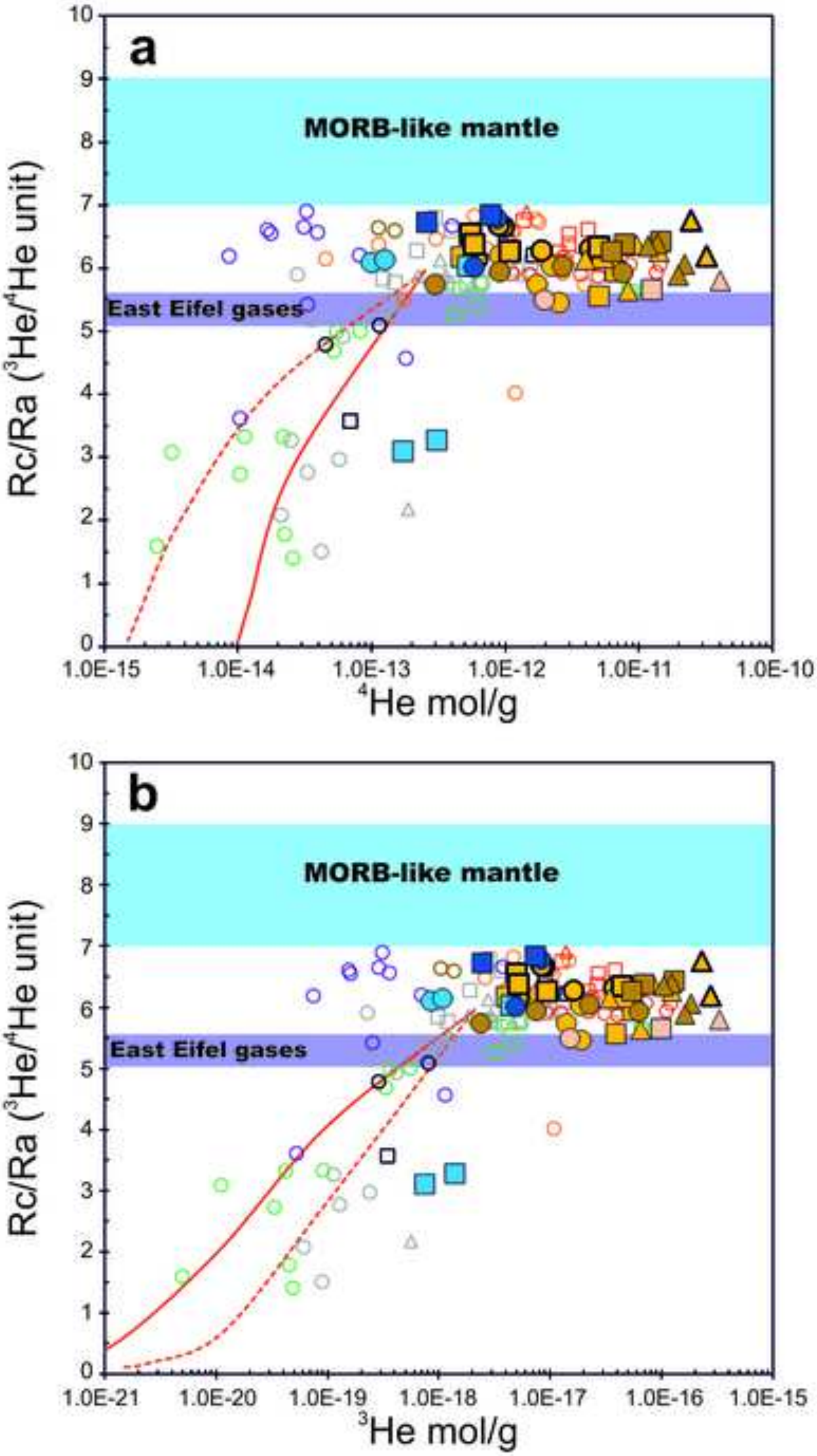
a
MORB-like mantle
East Eifel gases
Rc/Ra ($^3He/^4He$ unit)
^4He mol/g
1.0E-15
1.0E-14
1.0E-13
1.0E-12
1.0E-11
1.0E-10
b
MORB-like mantle
East Eifel gases
Rc/Ra ($^3He/^4He$ unit)
^3He mol/g
1.0E-21
1.0E-20
1.0E-19
1.0E-18
1.0E-17
1.0E-16
1.0E-15

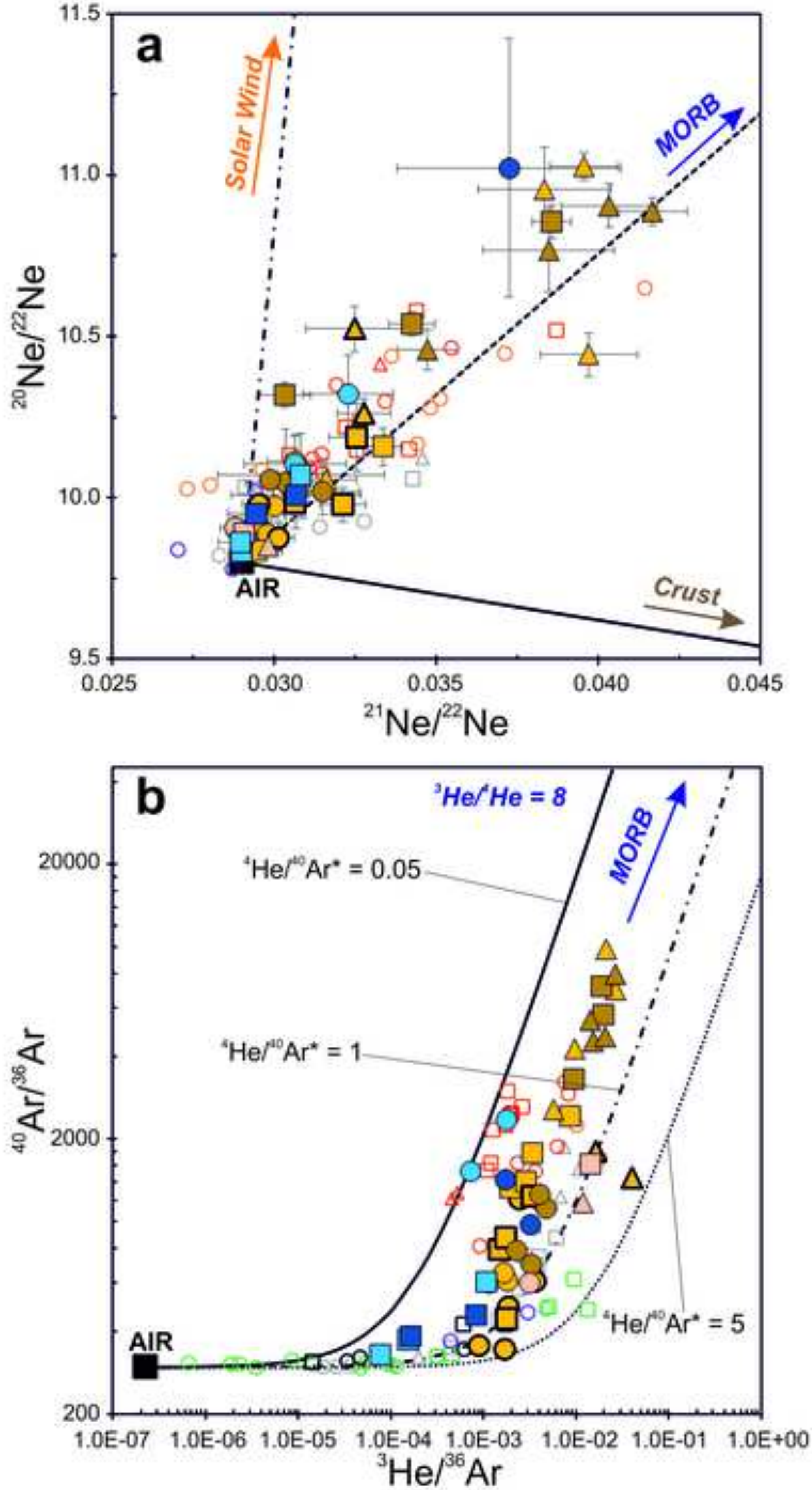
a
Solar Wind
MORB
AIR
Crust
^{20}Ne/^{22}Ne
^{21}Ne/^{22}Ne
11.5
11.0
10.5
10.0
9.5
0.025
0.030
0.035
0.040
0.045
b
^{3}He/^{4}He = 8
MORB
^{4}He/^{40}Ar* = 0.05
^{4}He/^{40}Ar* = 1
^{4}He/^{40}Ar* = 5
AIR
^{40}Ar/^{36}Ar
^{3}He/^{36}Ar
20000
2000
200
1.0E-07
1.0E-06
1.0E-05
1.0E-04
1.0E-03
1.0E-02
1.0E-01
1.0E+00

Figure 10

Click here to access/download;Figure;Figure 10.tif

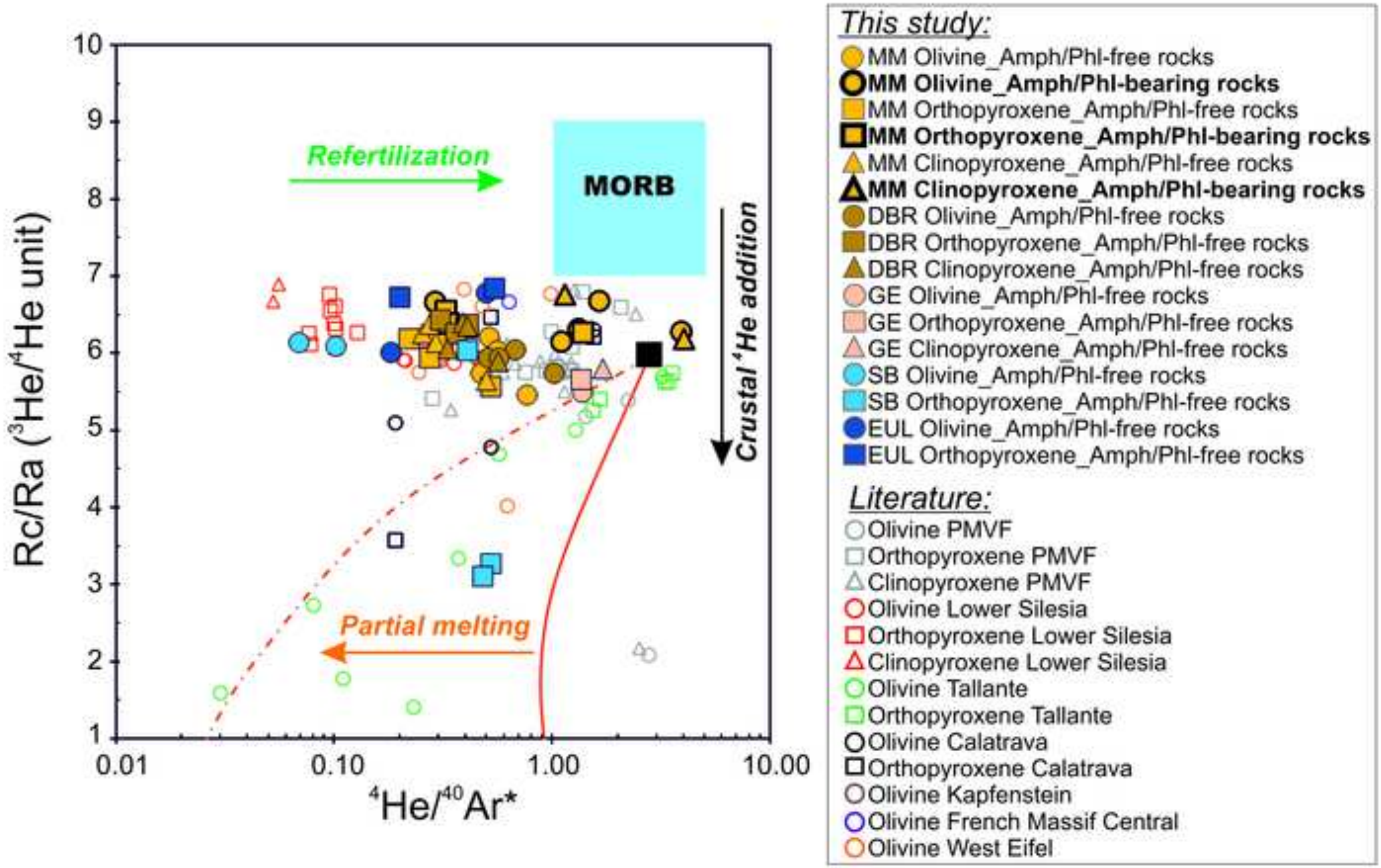

Figure 11

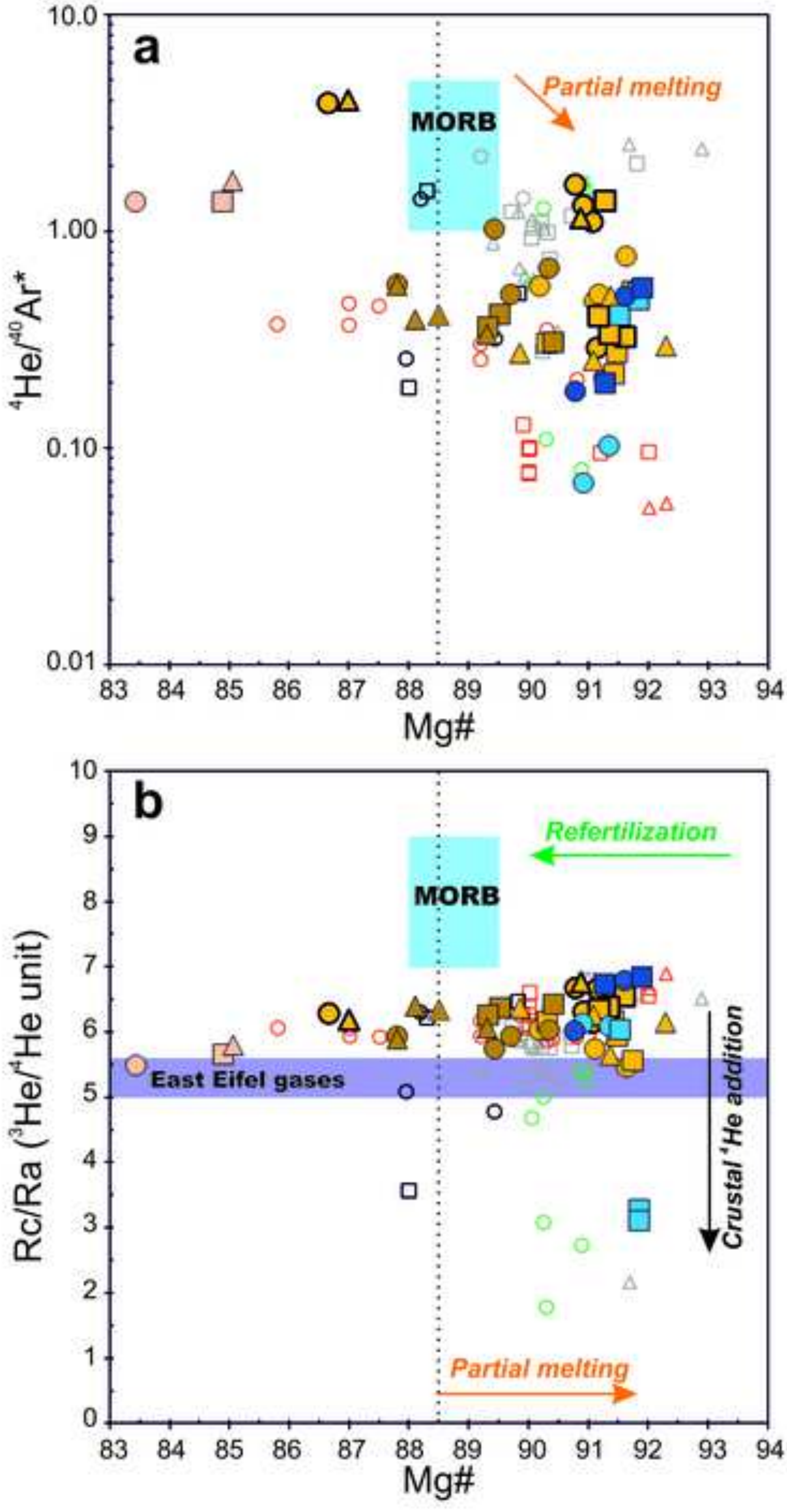

a
Partial melting
MORB
10.0
1.00
0.10
0.01
^{4}He/^{40}Ar*
83 84 85 86 87 88 89 90 91 92 93 94
Mg#
b
Refertilization
MORB
East Eifel gases
Crustal ^{4}He addition
Partial melting
0 1 2 3 4 5 6 7 8 9 10
Rc/Ra (^{3}He/^{4}He unit)
83 84 85 86 87 88 89 90 91 92 93 94
Mg#

Figure 12

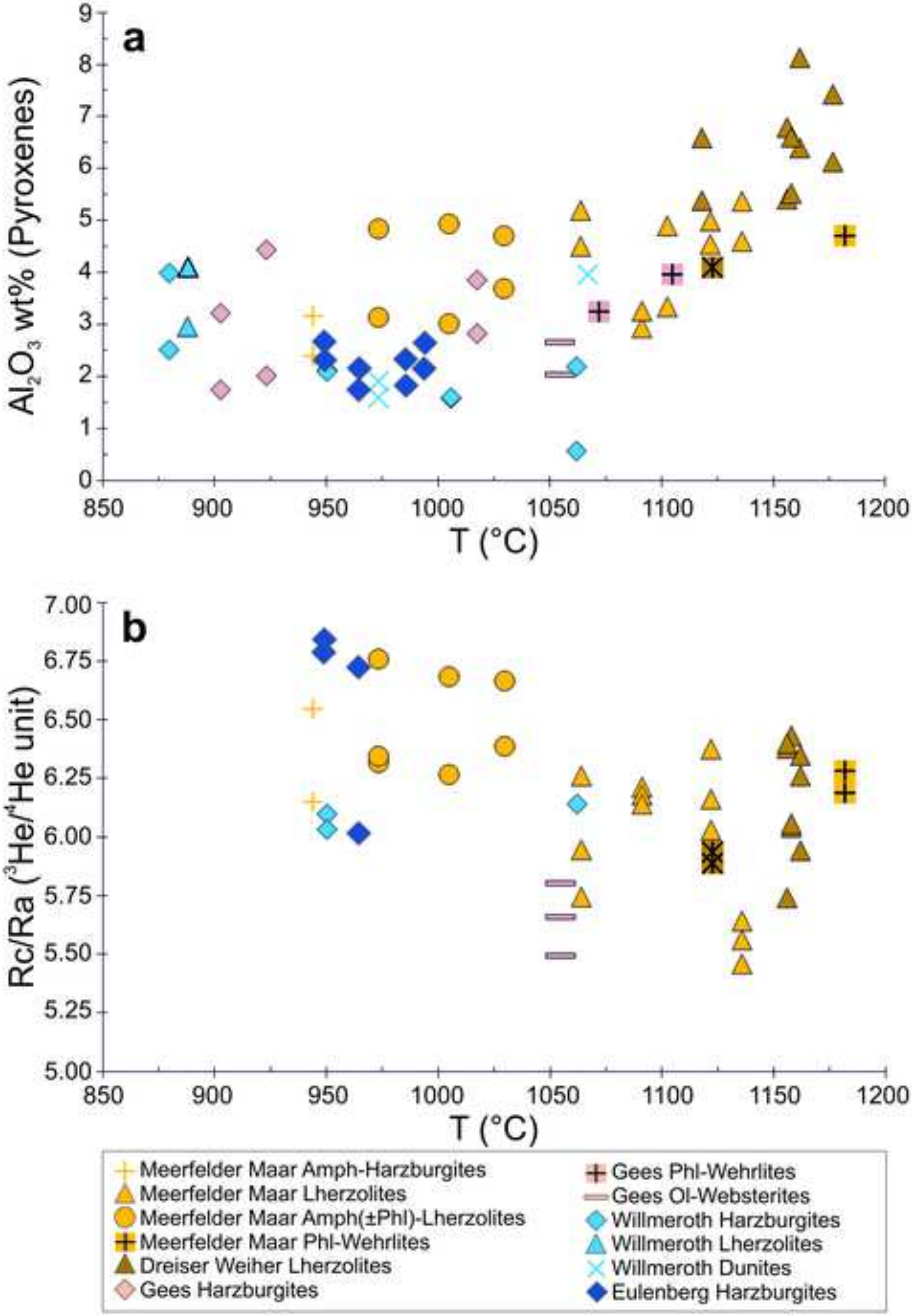

a
Al2O3 wt% (Pyroxenes)
T (°C)
b
Rc/Ra (3He/4He unit)
T (°C)
Meerfelder Maar Amph-Harzburgites
Meerfelder Maar Lherzolites
Meerfelder Maar Amph(±Phl)-Lherzolites
Meerfelder Maar Phl-Wehrlites
Dreiser Weiher Lherzolites
Gees Harzburgites
Gees Phl-Wehrlites
Gees Ol-Websterites
Willmeroth Harzburgites
Willmeroth Lherzolites
Willmeroth Dunites
Eulenberg Harzburgites

Table 1. Location, classification and modal estimates of West Eifel and Siebengebirge ultramafic xenoliths. For each sample, the equilibrium temperature and oxygen fugacity are also reported together with the standard deviation (StD). Temperature was calculated by means of [1] Ballhaus et al. (1991) thermometer; oxygen fugacity was calculated by means of [2] Miller et al. (2016), [1] Ballhaus et al. (1991) and [3] Bryndzia and Wood (1990) oxybarometers. Lh, lherzolite; Hz, harzburgite; Weh, wehrlite; Ol-Cpxite, ol-clinopyroxenite; Ol-Wb, ol-websterite; Dn, dunite; Ol, olivine; Opx, orthopyroxene; Cpx, clinopyroxene; Sp, spinel; Amph, amphibole; Phl, phlogopite; tr, traces; [a] low-*T* alteration.

Volcanic Field	Locality	Sample	Rock type	Textural type	Modal abundances							Thermal and redox state							
					Ol	Opx	Cpx	Sp	Amph	Phl	Glass	T°C [1]	StD	ΔFMQ [2]	StD	ΔFMQ [1]	StD	ΔFMQ [3]	StD
West Eifel	Meerfelder Maar	MM1	Weh	Mosaic equigranular	83	0	10	1	0	6	tr	1182	13	-	-	1.16	0.07	-	-
West Eifel	Meerfelder Maar	MM2	Lh	Protogranular	68	23	6	1	1	0	0	1030	14	0.41	0.02	0.26	0.03	0.62	0.06
West Eifel	Meerfelder Maar	MM3	Lh	Protogranular	78	14	7	2	1	0	tr	1005	5	0.31	0.04	0.13	0.03	0.35	0.04
West Eifel	Meerfelder Maar	MM4	Lh	Protogranular, foliated	71	21	6	2	0	0	0	1064	13	0.16	0.07	-0.01	0.08	0.25	0.08
West Eifel	Meerfelder Maar	MM5	Hz	Protogranular-tabular equigranular	69	17	4	2	7	0	tr	944	5	0.91	0.08	0.74	0.07	0.97	0.07
West Eifel	Meerfelder Maar	MM6	Lh	Protogranular-mosaic equigranular	77	16	6	2	0	0	tr	1091	13	0.76	0.01	0.57	0.01	0.96	0.04
West Eifel	Meerfelder Maar	MM7	Lh	Protogranular, foliated	71	19	8	2	0	0	0	1136	6	0.08	0.04	-0.06	0.04	0.29	0.06
West Eifel	Meerfelder Maar	MM8	Lh	Protogranular-mosaic equigranular	72	17	8	2	1	1	tr	974	10	0.51	0.02	0.40	0.02	0.69	0.05
West Eifel	Meerfelder Maar	MM9	Lh	Protogranular	67	23	9	2	0	0	0	1122	9	0.14	0.03	0.05	0.03	0.41	0.05
West Eifel	Meerfelder Maar	MM10	Lh	Protogranular-tabular equigranular	77	15	6	2	0	0	tr	1102	22	0.31	0.06	0.16	0.07	0.43	0.08
West Eifel	Dreiser Wehier	DBR1 Pd	Lh	Protogranular	73	15	10	2	0	0	tr	1118	29	0.24	0.02	0.34	0.01	0.54	0.03
West Eifel	Dreiser Wehier	DBR1 Px	Ol-Cpxite	Adcumulitic	18	0	81	1	0	0	tr	-	-	-	-	-	-	-	-
West Eifel	Dreiser Wehier	DBR2	Weh	Recrystallized cumulitic	56	0	43	1	0	0	0	1123	15	-	-	0.59	0.02	-	-
West Eifel	Dreiser Wehier	DBR3	Lh	Protogranular	68	16	14	2	0	0	0	1177	13	0.01	0.03	0.04	0.04	0.32	0.07
West Eifel	Dreiser Wehier	DBR4	Weh	Tabular equigranular, highly impregnated	65	0	22	1	5	6	1	-	-	-	-	-	-	-	-
West Eifel	Dreiser Wehier	DBR5	Lh	Protogranular	62	21	15	2	0	0	0	1156	37	-0.12	0.05	-0.12	0.05	0.25	0.07
West Eifel	Dreiser Wehier	DBR6	Lh	Protogranular	76	18	6	1	0	0	0	1158	10	0.24	0.04	0.25	0.04	0.54	0.07
West Eifel	Dreiser Wehier	DBR7	Hz	Tabular equigranular	84	11	3	1	0	0	1	-	-	-	-	-	-	-	-
West Eifel	Dreiser Wehier	DBR8	Lh	Protogranular	55	25	17	3	0	0	0	-	-	-	-	-	-	-	-
West Eifel	Dreiser Wehier	DBR9	Lh	Protogranular	59	22	17	3	0	0	0	1162	16	-0.29	0.05	-0.25	0.03	0.18	0.08
West Eifel	Dreiser Wehier	DBR10 Pd	Lh	Protogranular	72	20	7	1	0	0	0	-	-	-	-	-	-	-	-
West Eifel	Dreiser Wehier	DBR10 Dn	Dn	Mosaic equigranular-adcumulitic	91	0	0	8	0	0	0	-	-	-	-	-	-	-	-
West Eifel	Dreiser Wehier	DBR11	Ol-Cpxite	Orthocumulitic	29	0	71	0	0	0	0	-	-	-	-	-	-	-	-
West Eifel	Gees	GE1	Ol-Wb	Orthocumulitic	17	49	32	2	0	0	tr	1055	19	0.91	0.03	1.48	0.01	1.04	0.04
West Eifel	Gees	GE2	Weh	Adcumulitic-infiltrated	82	0	16	1	0	1	tr	-	-	-	-	-	-	-	-
West Eifel	Gees	GE3	Hz	Porphyroclastic	71	23	4	1	0	0	tr	923	8	1.18	0.03	0.99	0.03	1.37	0.06
West Eifel	Gees	GE4	Hz	Porphyroclastic	75	19	5	2	0	0	0	1017	17	0.80	0.06	0.56	0.06	1.08	0.08
West Eifel	Gees	GE5	Weh	Adcumulitic-infiltrated	70	0	14	3	0	13	0	1105	11	-	-	1.69	0.33	-	-
West Eifel	Gees	GE6	Lh	Porphyroclastic	76	15	8	1	0	0	tr	-	-	-	-	-	-	-	-
West Eifel	Gees	GE7	Ol-Cpxte	Adcumulitic-infiltrated	57	0	42	1	0	0	tr	-	-	-	-	-	-	-	-
West Eifel	Gees	GE8	Weh	Adcumulitic-infiltrated	65	0	23	2	0	10	tr	-	-	-	-	-	-	-	-
West Eifel	Gees	GE9	Weh	Adcumulitic-infiltrated	77	0	22	1	0	tr	0	1072	66	-	-	0.32	0.17	-	-
West Eifel	Gees	GE10	Hz	Porphyroclastic	69	24	4	3	0	0	0	903	8	1.03	0.06	0.82	0.06	1.12	0.05
Siebengebirge	Willmeroth	SB1	Dn	Porphyroclastic, spinel aligned	89	8	2	2	0	0	tr [a]	973	5	0.92	0.21	0.78	0.25	1.08	0.23
Siebengebirge	Willmeroth	SB2	Hz	Porphyroclastic, spinel aligned	73	20	5	3	0	0	tr [a]	880	22	-0.45	0.62	-0.79	0.64	-0.22	0.63
Siebengebirge	Willmeroth	SB3	Hz	Porphyroclastic, spinel aligned	72	20	4	3	0	0	tr [a]	950	21	1.06	0.07	0.82	0.08	1.30	0.09
Siebengebirge	Willmeroth	SB4	Hz	Porphyroclastic	79	15	4	2	0	0	tr [a]	1006	26	0.85	0.22	0.60	0.27	0.92	0.25
Siebengebirge	Willmeroth	SB5	Hz	Porphyroclastic	72	25	3	1	0	0	tr [a]	1062	16	0.65	0.05	0.21	0.03	0.49	0.06
Siebengebirge	Willmeroth	SB6	Lh	Porphyroclastic	74	17	7	2	0	0	tr [a]	888	26	-0.09	0.43	-0.39	0.42	0.08	0.38
Siebengebirge	Willmeroth	SB7	Dn	Mosaic equigranular- II gen protogranular	93	0	6	1	0	0	tr [a]	1067	30	-	-	1.15	0.25	-	-
Siebengebirge	Willmeroth	SB9	Dn	Mosaic equigranular- II gen protogranular	92	0	7	1	0	0	tr [a]	-	-	-	-	-	-	-	-
Siebengebirge	Willmeroth	SB10	Hz	Porphyroclastic	79	19	1	2	0	0	tr [a]	-	-	-	-	-	-	-	-
Siebengebirge	Eulenberg	EUL1	Hz	Porphyroclastic	72	22	3	3	0	0	tr [a]	994	59	0.44	0.17	0.15	0.19	0.65	0.16
Siebengebirge	Eulenberg	EUL2	Hz	Porphyroclastic	76	20	3	2	0	0	tr [a]	965	20	0.52	0.03	0.30	0.03	0.80	0.05
Siebengebirge	Eulenberg	EUL3	Hz	Porphyroclastic	70	28	1	1	0	0	tr [a]	-	-	-	-	-	-	-	-
Siebengebirge	Eulenberg	EUL4	Hz	Porphyroclastic	74	20	4	2	0	0	tr [a]	986	20	0.54	0.08	0.30	0.08	0.71	0.16
Siebengebirge	Eulenberg	EUL5	Hz	Porphyroclastic	70	26	3	1	0	0	tr [a]	949	35	0.24	0.07	-0.08	0.10	0.38	0.13
Siebengebirge	Eulenberg	EUL6	Dn	Porphyroclastic	98	0	1	1	0	0	tr [a]	-	-	-	-	-	-	-	-
Siebengebirge	Eulenberg	EUL7	Hz	Porphyroclastic	66	29	4	1	0	0	tr [a]	-	-	-	-	-	-	-	-

Click here to access/download
Background dataset for online publication only
Supplementary Tables.xlsx

Declaration of interests

☒ The authors declare that they have no known competing financial interests or personal relationships that could have appeared to influence the work reported in this paper.

☐The authors declare the following financial interests/personal relationships which may be considered as potential competing interests: